

*The authors have done a thorough revision of the manuscript, and I would like to thank them for their efforts in accommodating all reviewer comments. In particular the additional model evaluation, improved discussion and change of title have substantially improved the manuscript. I agree with all responses, except for one thing: I do think that impacts of changing fuel load (driven by changing productivity) on fire emissions could be substantial, and could potentially alter the results - even if the uncertainties are currently too large to quantify the effect. For example, Knorr et al. (2016) found a large impact on fire emissions from increasing fuel load due to CO<sub>2</sub> fertilization - compensated by varying degrees by decreasing fuel load due to climate change (Fig. 5 there). Since both have substantial uncertainties, we have a situation with two large and uncertain effects compensating each other. The negative impact on fire emissions due to climate change simulated with a DGVM in that paper could be moderated through the aerosol impact on NPP the authors discuss in the present manuscript. This would then constitute a negative feedback loop, which could potentially dampen the impact of fire emissions on plant productivity. As said, I would like to see an additional discussion of this.*

*Knorr, W., Jiang, L., and Arneeth, A.: Climate, CO<sub>2</sub>, and demographic impacts on global wildfire emissions, *Biogeosci.*, 13, 267-282, doi:10.5194/bg-13-267-2016, 2016.*

RESPONSE: We thank the reviewer for helpful comments. The study of Knorr et al. (2016) mentioned by the reviewer actually supports our conclusion that prediction of future fuel load is very uncertain. On one hand, CO<sub>2</sub> fertilization may increase global vegetation carbon (hence fuel load). On the other hand, changes in climate and population may cause opposite trends in fuel load, offsetting CO<sub>2</sub> effects. Furthermore, fire prediction in Knorr et al. (2016) is performed based on DGVM, which is not evaluated against observations. Such deficit may introduce uncertainties to the foundation of projection but is hard to quantify. Taken all these together, we consider our assumption of constant fuel load is logically sound, and we have discussed the related uncertainties thoroughly.

In the revised paper, we include Knorr et al. (2016) paper and extend our discussion about uncertainty sources in the projection of fuel load as follows (see underlined words):

“On the contrary, projections using DGVMs show a widespread increase in vegetation carbon under the global warming scenario with CO<sub>2</sub> fertilization of photosynthesis (Friend et al., 2014; Knorr et al., 2016). In addition, compound factors such as greenhouse gas mitigation (Kim et al., 2017), population change (Knorr et al., 2016), pine beetle outbreak (Kurz et al., 2008), and fire management (Doerr and Santin, 2016) may exert varied impacts on future vegetation and fuel load.” (Lines 629-634)

1 **Future inhibition of ecosystem productivity by increasing wildfire pollution**  
2 **over boreal North America**

3

4 Xu Yue<sup>1</sup>, Susanna Strada<sup>2</sup>, Nadine Unger<sup>3</sup>, Aihui Wang<sup>4</sup>

5

6

7 <sup>1</sup> Climate Change Research Center, Institute of Atmospheric Physics, Chinese Academy of  
8 Sciences, Beijing 100029, China

9 <sup>2</sup> Laboratoire des Sciences du Climat et de l'Environnement, L'Orme des Merisiers - Bat 712,  
10 91191 Gif Sur Yvette, France

11 <sup>3</sup> College of Engineering, Mathematics and Physical Sciences, University of Exeter, Exeter,  
12 EX4 4QE, UK

13 <sup>4</sup> Nansen-Zhu International Research Centre, Institute of Atmospheric Physics, Chinese  
14 Academy of Sciences, Beijing 100029, China

15

16 *Corresponding author:*

17 Xu Yue

18 Telephone: 86-10-82995369

19 Email: xuyueseas@gmail.com

20

21 *Keywords:* wildfire emissions, ozone, aerosols, net primary productivity, climate change,  
22 diffuse fertilization effect, carbon loss, earth system modeling

23

24

25

26  
27  
28  
29  
30  
31  
32  
33  
34  
35  
36  
37  
38  
39  
40  
41  
42  
43  
44  
45  
46  
47  
48  
49  
50  
51  
52

### Abstract

Biomass burning is an important source of tropospheric ozone (O<sub>3</sub>) and aerosols. These air pollutants can affect vegetation photosynthesis through stomatal uptake (for O<sub>3</sub>) and light scattering and absorption (for aerosols). Wildfire area burned is projected to increase significantly in boreal North America by the midcentury, while little is known about the impacts of enhanced emissions on the terrestrial carbon budget. Here, combining site-level and satellite observations and a carbon-chemistry-climate model, we estimate the impacts of fire emitted O<sub>3</sub> and aerosols on net primary productivity (NPP) over boreal North America. Fire emissions are calculated based on an ensemble projection from 13 climate models. In the present day, wildfire enhances surface O<sub>3</sub> by 2 ppbv (7%) and aerosol optical depth (AOD) at 550 nm by 0.03 (26%) in the summer. By midcentury, area burned is predicted to increase by 66% in boreal North America, contributing more O<sub>3</sub> (13%) and aerosols (37%). Fire O<sub>3</sub> causes negligible impacts on NPP because ambient O<sub>3</sub> concentration (with fire contributions) is below the damage threshold of 40 ppbv for 90% summer days. Fire aerosols reduce surface solar radiation but enhance atmospheric absorption, resulting in enhanced air stability and intensified regional drought. The domain of this drying is confined to the North in the present day, but extends southward by 2050 due to increased fire emissions. Consequently, wildfire aerosols enhance NPP by 72 Tg C yr<sup>-1</sup> in the present day but decrease NPP by 118 Tg C yr<sup>-1</sup> in the future, mainly because of the soil moisture perturbations. Our results suggest that future wildfire may accelerate boreal carbon loss, not only through direct emissions increasing from 68 Tg C yr<sup>-1</sup> at present day to 130 Tg C yr<sup>-1</sup> by midcentury, but also through the biophysical impacts of fire aerosols.

## 53 **1 Introduction**

54

55 Wildfire area burned is increasing in recent decades over North America boreal regions  
56 (Stocks et al., 2002; Kasischke and Turetsky, 2006). Fire activity is closely related to weather  
57 conditions and large-scale atmospheric oscillations (Gillett et al., 2004; Duffy et al., 2005),  
58 and is projected to increase significantly in the future due to climatic changes (Flannigan et  
59 al., 2005; Balshi et al., 2009; Groot et al., 2013; Wang et al., 2015). More area burned and the  
60 consequent fire emissions are accelerating carbon loss in boreal North America (Bond-  
61 Lamberty et al., 2007; Turetsky et al., 2011). Meanwhile, fire-induced air pollution, including  
62 ozone (O<sub>3</sub>) and aerosols, is predicted to increase in boreal and downwind regions by  
63 midcentury (Yue et al., 2013; Yue et al., 2015). Wildfire emissions have large impacts on air  
64 quality (Wotawa and Trainer, 2000; Morris et al., 2006), weather/climate conditions  
65 (Randerson et al., 2006; Zhao et al., 2014), and public health (Zu et al., 2016; Liu et al.,  
66 2017). However, little is known about how these pollutants affect ecosystem carbon  
67 assimilation, and how this impact will change with the increased wildfire activity in the  
68 future.

69

70 Surface O<sub>3</sub> causes damages to photosynthesis through stomatal uptake (Sitch et al., 2007). In  
71 the present climate state, fire-induced O<sub>3</sub> enhancements are predicted to reduce net primary  
72 productivity (NPP) in the Amazon forest by 230 Tg C yr<sup>-1</sup> (1 Tg = 10<sup>12</sup> g), a magnitude  
73 comparable to the direct release of CO<sub>2</sub> from fires in South America (Pacífico et al., 2015).  
74 The aerosol effects are more uncertain because both positive and negative feedbacks occur.  
75 Appearance of aerosols increases diffuse light, which is beneficial for shaded leaves in the  
76 lower canopy. Consequently, photosynthesis of the whole ecosystem will increase as long as  
77 the total light availability is not compromised (Kanniah et al., 2012). Rap et al. (2015)  
78 estimated that biomass burning aerosols increase Amazon NPP by 78–156 Tg C yr<sup>-1</sup>, which  
79 offsets about half of the damage caused by fire O<sub>3</sub> (Pacífico et al., 2015). In contrast, strong  
80 light attenuation associated with high aerosol loading may decrease canopy photosynthesis  
81 (Cohan et al., 2002; Oliveira et al., 2007; Cirino et al., 2014). Furthermore, the aerosol  
82 radiative effects indirectly influence ecosystem productivity through concomitant  
83 meteorological perturbations that are only beginning to be examined (Yue et al., 2017).

84

85 Future wildfire activity is projected to increase over boreal North America but with large  
86 uncertainties (Flannigan et al., 2005; Tymstra et al., 2007; Girardin and Mudelsee, 2008;  
87 Nitschke and Innes, 2008; Amiro et al., 2009; Balshi et al., 2009; Bergeron et al., 2010;  
88 Wotton et al., 2010; de Groot et al., 2013; Wang et al., 2016). For example, Amiro et al.  
89 (2009) predicted an increase of 34% in Canadian area burned for a 2×CO<sub>2</sub> scenario (2040-  
90 2060) relative to a 1×CO<sub>2</sub> condition (1975-1995), using the Canadian Fire Weather Index  
91 (CFWI) and output from Canadian global climate model (CGCM) version 1. Balshi et al.  
92 (2009) projected that area burned in boreal North America would double by the year 2045-  
93 2050 relative to 1991-2000, using the Multivariate Adaptive Regression Splines (MARS)  
94 approach and meteorological output from CGCM version 2. The increasing rate in Balshi et  
95 al. (2009) is higher than that in Amiro et al. (2009), indicating substantial uncertainties in fire  
96 projections originating from both fire models and simulated future climate. However, even  
97 with the same fire models and climate change scenario, large uncertainties (in both  
98 magnitude and signs) are found in the projection of area burned among individual climate  
99 models (Moritz et al., 2012; Yue et al., 2013). The multi-model ensemble approach has  
100 shown superior predictability over single models in historical climate simulations (Flato et al.,  
101 2013) and near-term climate predictions (Kirtman et al., 2014), and has been used as a  
102 standard technique to assess changes of climate variables in the long-term projections  
103 (Collins et al., 2013). Following this strategy, Yue et al. (2015) used output from 13 climate  
104 models to drive fire regression models and predicted an average increase of 66% in boreal  
105 area burned at 2046-2065 relative to 1981-2000 under the IPCC A1B scenario (Solomon et  
106 al., 2007). Yue et al. (2015) further calculated that the wildfire emission increase by the  
107 2050s would increase mean summertime surface O<sub>3</sub> by 5 ppbv in Alaska and 3 ppbv in  
108 Canada. The study found regional maximum O<sub>3</sub> enhancements as high as 15 ppbv, suggesting  
109 the potential for possible vegetation damage and land carbon loss due to the enhanced boreal  
110 fire-related air pollution. Wildfire aerosols are also expected to increase significantly but not  
111 predicted in Yue et al. (2015).

112

113 In this study, we quantify the impacts of O<sub>3</sub> and aerosols emitted from boreal wildfires on the  
114 land carbon uptake in North America in the present climate state and in the future world at  
115 2050, taking advantage of the ensemble projection of future wildfire emissions by Yue et al.  
116 (2015). The major chain we investigate includes i) generation of aerosols and surface ozone  
117 from wildfire emissions and ii) impact of fire-emitted aerosols and ozone on plant

118 photosynthesis through physical and biogeochemical processes (Fig. 1). We first analyze  
119 relationships between gross primary production (GPP) and aerosol optical depth (AOD) at  
120 550 nm over the boreal regions based on observations. We then perform a suite of Earth  
121 system model simulations using NASA GISS ModelE2 that embeds the Yale Interactive  
122 Terrestrial Biosphere model (YIBs), a framework known as ModelE2-YIBs (Yue and Unger,  
123 2015). Future projections of wildfire emissions from Yue et al. (2015) are applied as input to  
124 ModelE2-YIBs model to project fire-induced O<sub>3</sub> and aerosol concentrations in the 2010s and  
125 2050s. The impacts of the boreal fire O<sub>3</sub> on forest photosynthesis are predicted using the flux-  
126 based damage algorithm proposed by Sitch et al. (2007), which has been fully evaluated  
127 against available O<sub>3</sub> damage sensitivity measurements globally and over North America (Yue  
128 and Unger, 2014; Yue et al., 2016; Yue et al., 2017). Fire aerosols induce perturbations to  
129 radiation, meteorology, and hydrology, leading to multiple influences on the land carbon  
130 uptake. Sensitivity experiments are performed using the YIBs model in offline mode to  
131 isolate the contributions of changes in the individual meteorological drivers.

132

133

## 134 **2 Materials and methods**

135

### 136 **2.1 Observed GPP-AOD relationships**

137

138 Following the approach by Strada et al. (2015), we investigate the GPP sensitivity to diffuse  
139 radiation and AOD variability in boreal regions. First, we identify study sites in Canada and  
140 Alaska from the AmeriFlux (AMF) network (<http://ameriflux.lbl.gov/>). There are much fewer  
141 boreal sites than those in temperate regions. We select AMF sites providing hourly (or half-  
142 hourly) simultaneous measurements of GPP (non gap-filled) and photosynthetically active  
143 radiation (PAR, total and diffuse) for at least 3 consecutive years. Only two Canadian sites  
144 meet the criteria: Groundhog River (CA-Gro, 82.2°W, 48.2°N), a mixed forest (MF), and  
145 Quebec Mature Boreal Forest Site (CA-Qfo, 73.4°W, 49.7°N), an evergreen needleleaf forest  
146 (ENF). At the two selected sites, we calculate the Pearson's correlation coefficients between  
147 half-hourly GPP and different components of PAR. In total, we select 2432 and 3201 pairs of  
148 GPP and PAR measurements at CA-Gro and CA-Qfo, respectively. We then apply  
149 instantaneous Level 2 Collection 6 of AOD pixels at 3-km resolution retrieved by the  
150 Moderate Resolution Imaging Spectroradiometer (MODIS, <https://ladsweb.nascom.nasa.gov/>)

151 onboard the Aqua and Terra satellites (Levy et al., 2013). The MODIS 3-km AOD product  
152 has been fully validated against ground-based sun photometers at both global (Remer et al.,  
153 2013) and urban/suburban (Munchak et al., 2013) scales. Strada et al. (2015) used ground-  
154 based AOD observations from the Aerosol Robotic Network (AERONET) near AMF sites to  
155 validate the sampling technique of MODIS 3-km AOD product. They found high correlations  
156 of 0.89-0.98 and regression slopes from 0.89 to 1.03 for daily AOD between AERONET and  
157 MODIS at four AMF sites. For this study, the validation against ground-based AOD  
158 observations was not possible because no AERONET stations exist near to the selected AMF  
159 sites.

160

161 Every day, MODIS satellite sensors pass a specific region between 10:00 and 14:00 Local  
162 Time (LT), leaving patchy signals around the AmeriFlux sites. Most of MODIS AOD data at  
163 high latitudes are available only in boreal summer; as a result, we narrow our explorations of  
164 the GPP-AOD relationships to the noontime (10:00-14:00 LT) from June to August. The  
165 chosen noontime window limits the contributions that confounding factors such as low solar  
166 angles and high diffuse fraction may have on the amount of diffuse PAR and plant  
167 productivity (Niyogi et al., 2004). For each summer day, we select instantaneous MODIS 3-  
168 km AOD pixels that are (a) located within a distance of  $0.03^\circ$  (about 3 km) from the targeted  
169 AMF site and (b) “quasi-coincident” with AMF data, which are available each half-hour.  
170 Because of the unavoidable temporal differences between MODIS overpass and AMF data  
171 availability, we name this selection “quasi-coincident”. A cloud mask applied to the MODIS  
172 retrieval procedure conveniently filters out cloudy instants and should reduce the effect of  
173 clouds in the scattering process. We calculate both the correlation and regression coefficients  
174 between “quasi-coincident” GPP and AOD at the selected sites. Negative GPP is considered  
175 as a missing value. To further reduce the influence of cloud cover, we discard instants (both  
176 AMF and MODIS data) when precipitation is non-zero. In total, we select 65 pairs of GPP  
177 and AOD at CA-Gro site and another 59 pairs at CA-Qfo site. The GPP-AOD sampling pairs  
178 are much fewer than GPP-PAR, because we select instants when both instantaneous AOD  
179 and GPP data are available. In addition, AOD is screened for clear instants to exclude the  
180 impacts of clouds.

181

## 182 **2.2 Wildfire emissions**

183

184 Wildfire emissions used in climate modeling are calculated as the product of area burned,  
185 fuel consumption, and emission factors. To predict area burned, we build stepwise  
186 regressions for area burned in 12 boreal ecoregions (Yue et al., 2015). Observed area burned  
187 aggregated from inter-agency fire reports is used as the predictand. Predictors are selected  
188 from 44 ( $5 \times 6 + 7 \times 2$ ) variables including five meteorological parameters (mean and maximum  
189 temperature, relative humidity, precipitation, and geopotential height at 500 hPa) of six  
190 different time intervals (winter, spring, summer, autumn, fire season (May-October), and the  
191 whole year), as well as the mean and maximum values of 7 fire indexes from the CFWI  
192 system during fire season. We consider the impacts of antecedent factors on current fire  
193 activity by including all above variables at the same year and those in the previous two years,  
194 making a total of 132 ( $44 \times 3$ ) factors. The final formats of regression are different among  
195 ecoregions, depending on the selection of the factors that contribute the maximum observed  
196 variance in predictand but remain the minimum collinearity among predictors. These  
197 regression functions are then driven with output from 13 Coupled Model Intercomparison  
198 Project Phase 3 (CMIP3) climate models under A1B scenario (Meehl et al., 2007) to predict  
199 area burned at present day (1981-2000) and midcentury (2046-2065). In the A1B scenario,  
200 CO<sub>2</sub> concentration is projected to 532 ppm by the year 2050, similar to the value of 541 ppm  
201 in IPCC RCP8.5 scenario (van Vuuren et al., 2011) archived for the Coupled Model  
202 Intercomparison Project Phase 5 (CMIP5).

203

204 We derive  $1^\circ \times 1^\circ$  gridded area burned based on the prediction for each ecoregion following  
205 the approach by Yue et al. (2015). Temporally, the annual area burned estimated with  
206 regressions is first converted to monthly area burned using the mean seasonality for each  
207 boreal ecoregion during 1980-2009. Spatially, large fires tend to burn in ecosystems where  
208 historical fires are frequent because of favorable conditions (Keane et al., 2008). In each  $1^\circ \times 1^\circ$   
209 grid square, we calculate the frequency of large fires ( $>1000$  ha) during 1980-2009; these  
210 fires account for about 85% of total area burned in boreal North America. We arbitrarily  
211 attribute 85% of area burned within each ecoregion to a number of fires with fixed size of  
212 1000 ha. We then allocate these large fires among the  $1^\circ \times 1^\circ$  grid cells based on the observed  
213 spatial probability of large fires. For example, if one grid box (named grid 'A') bears 1% of  
214 large fires ( $>1000$  ha) within an ecoregion at present day, the same grid will bear the same  
215 possibility for large fires in the future. On the other hand, fuel availability limits reburning  
216 and fire spread during the forest return interval, suggesting that current burning will decrease



217 the possibility of future fires in the same location. To consider such impact, we scale the  
218 observed probabilities by the fraction remaining unburned in each grid box, and then use this  
219 modified probability distribution to allocate large fires for the remaining months. For  
220 example, if present-day fires have consumed 20% of the total area within the grid 'A', then  
221 the possibility of large fire will be 0.8% ( $1\% \times 0.8$ , instead of 1%) for this grid. Finally, we  
222 disaggregate the remaining 15% of area burned into fires 10 ha in size, and randomly  
223 distribute these fires across all grid boxes in the ecoregion. With this method, we derive the  
224 gridded area burned for boreal North America by eliminating reburning issues. Sensitivity  
225 tests show that specifying different area burned to the large fires (100 or 10 000 ha rather  
226 than 1000 ha) yields  $< 1\%$  changes in predicted biomass burned, suggesting that this  
227 approach is not sensitive to the presumed fire size in the allocation procedure.

228

229 Fuel consumption, the dry mass burned per fire area, is the product of fuel load and burning  
230 severity. For fuel load in Alaska, we use 1-km inventory from the US Forest Service (USFS)  
231 Fuel Characteristic Classification System (FCCS, McKenzie et al., 2007). For fuel load in  
232 Canada, we use a 1-km fuel type map from the Canadian Fire Behavior Prediction (FBP)  
233 system (Nadeau et al., 2005), combined with fuel-bed definition from the FCCS. Burning  
234 severity, the fraction of fuel load burned by fires, is calculated with the USFS CONSUME  
235 model 3.0 following the approach described in Val Martin et al. (2012). With both fuel load  
236 and burning severity, we derive fuel consumption and further calculate biomass burned in  
237 boreal North America with the predicted area burned. As in Amiro et al. (2009) and Yue et al.  
238 (2015), we apply constant fuel load for both present day and midcentury because opposite  
239 and uncertain factors influence future projections (Kurz et al., 2008; Heyder et al., 2011;  
240 Friend et al., 2014; Knorr et al., 2016; Kim et al., 2017). Instead, we consider changes in  
241 burning severity due to perturbations in fuel moisture as indicated by CFWI indexes (Yue et  
242 al., 2015). On average, we estimate a 9% increase in fuel consumption over boreal North  
243 America by the midcentury, because higher temperature and lower precipitation result in a  
244 future with drier fuel load (Flannigan et al., 2016).

245

246 Fire emissions for a specific species are then estimated as the product between biomass  
247 burned and the corresponding emission factor, which is adopted from measurements by  
248 Andreae and Merlet (2001) except for  $\text{NO}_x$ . We use the average value of 1.6 g NO per Kg dry  
249 mass burned (DM) from six studies as  $\text{NO}_x$  emission factor, because the number of 3.0 g NO

Xu Yue 10/11/17 11:07 PM

**Deleted:** (Kurz et al., 2008; Heyder et al., 2011; Friend et al., 2014; Kim et al., 2017)

252 per Kg DM reported in Andreae and Merlet (2001) is much higher than that of 1.1 g NO per  
253 Kg DM from field observations (Alvarado et al., 2010). Based on projected area burned and  
254 observation-based fuel consumption and emission factors, we derive fire emissions of NO<sub>x</sub>,  
255 carbon monoxide (CO), non-methane volatile organic compounds (NMVOCs, Alkenes and  
256 Alkanes), NH<sub>3</sub>, SO<sub>2</sub>, black (BC) and organic carbon (OC) in the present day and midcentury.

257

### 258 **2.3 NASA ModelE2-YIBs model**

259

260 The NASA ModelE2-YIBs is an interactive climate-carbon-chemistry model, which couples  
261 the chemistry-climate model NASA ModelE2 (Schmidt et al., 2014) and the YIBs vegetation  
262 model (Yue and Unger, 2015). NASA ModelE2 is a general circulation model with  
263 horizontal resolution of 2°×2.5° latitude by longitude and 40 vertical layers up to 0.1 hPa. It  
264 dynamically simulates both the physical (emissions, transport, and deposition) and chemical  
265 (production, conversion, and loss) processes of gas-phase chemistry (NO<sub>x</sub>, HO<sub>x</sub>, O<sub>x</sub>, CO, CH<sub>4</sub>,  
266 and NMVOCs), aerosols (sulfate, nitrate, ammonium, BC, OC, dust, and sea salt), and their  
267 interactions. In the model, oxidants influence the photochemical formation of secondary  
268 aerosol species (e.g., sulfate, nitrate, and biogenic secondary organic aerosol), in turn,  
269 aerosols alter photolysis rates and influence the online gas-phase chemistry. Size-dependent  
270 optical parameters computed from Mie scattering, including extinction coefficient, single  
271 scattering albedo, and asymmetry parameters, are applied for each aerosol type (Schmidt et  
272 al., 2014). The model also considers interactions between climate and atmospheric  
273 components. Simulated climate affects formation, transport, and deposition of atmospheric  
274 components, in turn, both O<sub>3</sub> and aerosols influence climate by altering radiation, temperature,  
275 precipitation, and other climatic variables. Both observation-based evaluations and multi-  
276 model inter-comparisons indicate that ModelE2 demonstrates skill in simulating climatology  
277 (Schmidt et al., 2014), soil moisture (Fig. S1), radiation (Wild et al., 2013), atmospheric  
278 composition (Shindell et al., 2013b), and radiative effects (Shindell et al., 2013a).

279

280 YIBs is a process-based vegetation model that dynamically simulates changes in leaf area  
281 index (LAI) through carbon assimilation, respiration, and allocation for prescribed PFTs.  
282 Coupled photosynthesis-stomatal conductance is simulated with the Farquhar-Ball-Berry  
283 scheme (Farquhar et al., 1980; Ball et al., 1987). Leaf-level photosynthesis is upscaled to  
284 canopy level by separating diffuse and direct light for sunlit and shaded leaves (Spitters,

285 1986). Plant respiration considers thermal dependence as well as acclimation to temperature  
286 (Atkin and Tjoelker, 2003). Soil respiration is calculated based on the carbon flows among 12  
287 biogeochemical pools (Schaefer et al., 2008). Net carbon uptake is allocated among leaves,  
288 stems, and roots to support leaf development and plant growth (Cox, 2001). The YIBs model  
289 has been benchmarked against *in situ* GPP from 145 eddy covariance flux tower sites and  
290 satellite retrievals of LAI and phenology (Yue and Unger, 2015). An interactive flux-based  
291 O<sub>3</sub> damage scheme proposed by Sitch et al. (2007) is applied to quantify the photosynthetic  
292 responses to ambient O<sub>3</sub> (Yue and Unger, 2014). For this scheme, O<sub>3</sub> damaging level is  
293 dependent on excess O<sub>3</sub> stomatal flux within leaves, which is a function of ambient O<sub>3</sub>  
294 concentration, boundary layer resistance, and stomatal resistance. Reduction of  
295 photosynthesis is calculated on the basis of plant functional types (PFTs), each of which  
296 bears a range of low-to-high sensitivities to O<sub>3</sub> uptake.

297

298

## 299 **2.4 Simulations**

300

301 Using the NASA ModelE2-YIBs model, we perform 6 time-slice simulations, three for  
302 present-day (2010s) and three for midcentury (2050s), with atmosphere-only configuration to  
303 explore the impacts of fire emissions on NPP in boreal North America (Table 1). Simulations  
304 F10CTRL and F50CTRL turn off all fire emissions as well as O<sub>3</sub> vegetation damage for the  
305 2010s and 2050s, respectively. However, climatic feedbacks of aerosols from other sources  
306 (both natural and anthropogenic) and related photosynthetic responses are included.  
307 Simulations F10AERO and F50AERO consider the responses of plant productivity to  
308 perturbations in radiation and meteorology caused by aerosols, including emissions from  
309 wildfires and other sources, but do not include any O<sub>3</sub> vegetation damage. In contrast,  
310 simulations F10O3 and F50O3 calculate offline O<sub>3</sub> damage based on the simulated O<sub>3</sub> from  
311 all sources including fire emissions. For these simulations, reductions of GPP are calculated  
312 twice with either low or high O<sub>3</sub> sensitivity. However, both of these GPP changes are not fed  
313 back into the model to influence carbon allocation and tree growth. Plant respiration is  
314 changing in response to meteorological perturbations, either due to climate change or aerosol  
315 radiative effects. We assume no impact of O<sub>3</sub> damage to plant respiration and examine  
316 vegetation NPP, the net carbon uptake by biosphere, for the current study. The difference  
317 between AERO and CTRL runs isolates the impacts of fire aerosols on NPP, and the

318 difference between O3 and CTRL runs isolates O<sub>3</sub> vegetation damage caused by fire and non-  
319 fire emission sources.

320  
321 All simulations are conducted for 20 years and outputs for the last 15 years are used for  
322 analyses. The simulations apply sea surface temperatures (SSTs) and sea ice distributions  
323 from previous NASA GISS experiments under the IPCC RCP8.5 scenario (van Vuuren et al.,  
324 2011). Decadal average monthly-varying SST and sea ice of 2006-2015 are used as boundary  
325 conditions for present-day (2010s) runs while that of 2046-2055 are used for future (2050s)  
326 runs. In the RCP8.5 scenario, global average SST increases by 0.62 °C while sea ice area  
327 decreases by 13.8% at the midcentury compared to the present-day level. Decadal average  
328 well-mixed greenhouse gas concentrations and anthropogenic emissions of short-lived  
329 species, both at present day and midcentury, are adopted from the RCP8.5 scenario (Table 2).  
330 The enhancement of CO<sub>2</sub> will affect climate (through longwave absorption) and ecosystem  
331 productivity (through CO<sub>2</sub> fertilization), but not the fire activity and related emissions  
332 directly. Natural emissions of soil and lightning NO<sub>x</sub>, biogenic volatile organic compounds  
333 (BVOC), dust, and sea salt are climate-sensitive and simulated interactively. The YIBs  
334 vegetation model cannot simulate changes in PFT fractions. The RCP8.5 land cover change  
335 dataset shows limited changes in land cover fractions between 2010s and 2050s (Oleson et al.,  
336 2010). For example, relative to the 2010s, a maximum gain of 5% is predicted for grassland  
337 in the 2050s, resulting from a 1% loss in deciduous forest and another 1% loss in needleleaf  
338 forest over boreal North America. As a result, a land cover dataset derived from satellite  
339 retrievals (Hansen et al., 2003) is applied as boundary conditions for both the 2010s and  
340 2050s.

341  
342 To evaluate the simulated GPP responses to changes in diffuse radiation, we perform site-  
343 level simulations using standalone YIBs model, which is driven with observed hourly  
344 meteorology (including temperature, relative humidity, surface pressure, wind speed, and soil  
345 moisture) and both diffuse and direct PAR at sites CA-Gro and CA-Qfo. To isolate the  
346 impact of individual aerosol-induced climatic perturbations on NPP, we perform 10  
347 sensitivity experiments using the offline YIBs model driven with offline meteorology  
348 simulated by ModelE2-YIBs model (Table 3). For example, the offline run Y10\_CTRL is  
349 driven with variables from the online simulation of F10CTRL (Table 1). The run Y10\_TAS  
350 adopts the same forcing as Y10\_CTRL except for temperature, which is simulated by the  
351 climate simulation of F10AERO. In this case, we quantify the NPP responses to individual

352 and/or combined climate feedback (mainly in temperature, radiation, and soil moisture) by  
353 fire aerosols. Each offline run is conducted for 12 years and the last 10 years are used for  
354 analyses.

355

## 356 **2.5 Observation datasets**

357

358 We use observations to evaluate GPP, AOD, and O<sub>3</sub> in boreal North America simulated by  
359 ModelE2-YIBs. For GPP, we use a benchmark data product upscaled from FLUXNET eddy  
360 covariance data using an ensemble of regression trees (Jung et al., 2009). For AOD  
361 observations, we use satellite retrieval at 550 nm from Terra MODIS Level 3 data product.  
362 For O<sub>3</sub>, gridded datasets are not available. We use site-level observations from 81 U.S. sites  
363 at the Clean Air Status and Trends Network (CASTNET, <https://www.epa.gov/castnet>) and  
364 202 Canadian sites at the National Air Pollution Surveillance (NAPS,  
365 <http://www.ec.gc.ca/rnsps-naps/>) program. All datasets are averaged over the 2008-2012  
366 period to represent present-day climatological conditions. Gridded datasets are interpolated to  
367 the same 2°×2.5° resolution as ModelE2-YIBs model.

368

369

## 370 **3 Results**

371

### 372 **3.1 Observed GPP-AOD relationships**

373

374 Positive correlations between GPP and diffuse PAR are found at the two boreal sites (Figs  
375 2b-2c). The magnitude of diffuse PAR is similar for these sites, possibly because they are  
376 located at similar latitudes (Fig. 2a). GPP values at CA-Gro are generally higher than that at  
377 CA-Qfo, likely because deciduous broadleaf forest (DBF) has higher photosynthetic rates.  
378 Consequently, the slope of regression between GPP and PAR<sub>dir</sub> is higher at CA-Gro than that  
379 at CA-Qfo, suggesting that GPP of DBF (or MF) is more sensitive to changes in diffuse PAR  
380 than that of ENF. We find almost zero correlation between GPP and PAR<sub>dir</sub> at the two sites  
381 (Table 4), indicating that photosynthesis is in general light-saturated for sunlit leaves at these  
382 sites during boreal summer noontime. As a result, modest reductions in direct light by  
383 aerosols will not decrease GPP of the whole canopy.

384

385 With satellite-based AOD, we find positive correlations between GPP and AOD at both sites  
386 (Figs 2d-2e). However, the slope of regression between GPP and AOD is lower (and not  
387 significant) at CA-Gro compared with that at CA-Qfo, opposite to the GPP-PAR<sub>dir</sub>  
388 regressions. The cause of such discrepancy might be related to the limitation of data  
389 availability. For the same reason, the GPP-AOD correlation is insignificant at CA-Gro site.  
390 On average, GPP sensitivity (denoted as mean  $\pm$  range) is estimated as  $3.5 \pm 1.1 \mu\text{mol m}^{-2} \text{s}^{-1}$   
391 per unit AOD at lower latitudes of boreal regions in the summer.

392

### 393 **3.2 Model evaluations**

394

395 Simulated summer GPP shows high values in mid-western Canada (Alberta and  
396 Saskatchewan) and the Southeast (Ontario) (Fig. 3a). Forest GPP at high latitudes is low  
397 because of the cool weather and light limitation there. Simulated GPP reasonably captures the  
398 spatial distribution with a high correlation coefficient of 0.77 ( $p \ll 0.01$ ) and relatively small  
399 biases within 20% of the data product. Simulated AOD reproduces the observed spatial  
400 pattern including the high values in boreal forests (Fig. 3b). In contrast to the MODIS  
401 observations, predicted AOD is relatively uniform over the West with a background value of  
402  $\sim 0.1$ . This discrepancy explains the low correlation coefficient ( $R = 0.25$ ,  $p < 0.01$ ) between  
403 the model and MODIS data. The simulation fails to capture the high values in the west,  
404 possibly due to a climate model underestimation of biogenic secondary organic aerosol,  
405 which may be an important contribution over the western boreal forest. Simulated maximum  
406 daily 8-hour average (MDA8) [O<sub>3</sub>] shows low values in boreal North America and high  
407 values in the western and eastern U.S. (Fig. 4a). This pattern is consistent with surface  
408 observations (Fig. 4b), but the model overestimates the measured surface O<sub>3</sub> by 22%. The  
409 Canadian measurement sites are located near the southern boundary, and as a result do not  
410 represent the average state over the vast boreal region at higher latitudes.

411

412 With the Sitch et al. (2007) scheme, the YIBs model simulates reasonable GPP responses to  
413 [O<sub>3</sub>] in North America (Yue and Unger, 2014; Yue et al., 2016). Generally, damage to GPP  
414 increases with the enhancement of ambient [O<sub>3</sub>], but with varied sensitivities for different  
415 plant species (see Fig. 6 of Yue and Unger (2014)). In responses to the same level of [O<sub>3</sub>],  
416 predicted O<sub>3</sub> damages are higher for deciduous trees than that for needleleaf trees, consistent  
417 with observations from meta-analyses (Wittig et al., 2007). The model also reproduces

418 observed light responses of GPP to diffuse radiation in boreal regions. With the site-level  
419 simulations, we evaluate the modeled GPP-PAR<sub>dif</sub> relationships at the hourly (instead of half-  
420 hourly) time step during summer. For 1342 pairs of GPP and PAR<sub>dif</sub> at the site CA-Gro, the  
421 observed correlation coefficient is 0.42 and regression slope is 0.011, while the results for the  
422 simulation are 0.60 and 0.014, respectively. At the site CA-Qfo, the observations yield a  
423 correlation coefficient of 0.46 and regression slope of 0.007 for 1777 pairs of GPP and  
424 PAR<sub>dif</sub>. The simulated correlation is 0.61 and the regression is 0.011 at the same site. The  
425 GPP sensitivity to PAR<sub>dif</sub> in the model is slightly higher than that of the available  
426 observations, likely because the latter are affected by additional non-meteorological abiotic  
427 factors. To remove the influences of compound factors other than radiation, we follow the  
428 approach of Mercado et al. (2009) to discriminate GPP responses to ‘diffuse’ and ‘direct’  
429 components of PAR at the two sites (Fig. 5). The model successfully reproduces the observed  
430 GPP-to-PAR sensitivities. Increase in PAR boosts GPP, but the efficiency is much higher for  
431 diffuse light than that for direct light, suggesting that increase of diffuse radiation is a benefit  
432 for plant growth.

433

### 434 **3.3 Simulation of wildfire O<sub>3</sub> and aerosols**

435

436 During 1980-2009, wildfire is observed to burn  $2.76 \times 10^6$  ha and 156.3 Tg DM every year  
437 over boreal North America. Similarly, the ensemble prediction with fire regression models  
438 estimates present-day area burned of  $2.88 \times 10^6$  ha yr<sup>-1</sup> and biomass burned of 160.2 Tg DM  
439 yr<sup>-1</sup> (Yue et al., 2015). By the midcentury, area burned is projected to increase by 77% (to  
440  $5.10 \times 10^6$  ha yr<sup>-1</sup>) in boreal North America, mainly because of the higher temperature in  
441 future fire seasons. Consequently, biomass burned increases by 93% (to 308.6 Tg DM yr<sup>-1</sup>)  
442 because fuel consumption also increases by 9% on average in a drier climate (Yue et al.,  
443 2015). Enhanced fire emissions increase concentrations of surface O<sub>3</sub> and column AOD,  
444 especially over Alaska and central Canada (Fig. 6). The maximum centers of air pollutants  
445 are collocated for O<sub>3</sub> and AOD but with unproportional magnitudes, suggesting non-linear  
446 conversion among fire emission species as well as the interactions with natural emission  
447 sources (e.g., lightning/soil NO<sub>x</sub> and BVOC). On average, wildfire emissions contribute  $7.1 \pm$   
448  $3.1\%$  ( $2.1 \pm 0.9$  ppbv) to surface O<sub>3</sub> and  $25.7 \pm 2.4\%$  ( $0.03 \pm 0.003$ ) to AOD in the summer  
449 over boreal North America in the present day. By midcentury, these ratios increase  
450 significantly to  $12.8 \pm 2.8\%$  ( $4.2 \pm 0.9$  ppbv) for O<sub>3</sub> and  $36.7 \pm 2.0\%$  ( $0.05 \pm 0.003$ ) for AOD.

451

### 452 3.4 Simulation of fire pollution impacts on NPP

453

454 Surface O<sub>3</sub>, including both fire and non-fire emissions (Table 2), causes limited (1-2%)  
455 damages to summer GPP in boreal North America (Fig. 7). The most significant damage is  
456 predicted over eastern U.S., where observed [O<sub>3</sub>] is high over vast forest ecosystems (Fig. 4).  
457 In the western U.S., [O<sub>3</sub>] is also high but the O<sub>3</sub>-induced GPP reduction is trivial because low  
458 stomatal conductance in the semi-arid ecosystems limits O<sub>3</sub> uptake there (Yue and Unger,  
459 2014). Over boreal North America, dominant PFTs are ENF (accounting for 44% of total  
460 vegetation cover) and tundra (treated as shrubland, accounting for 41% of total vegetation  
461 cover). Both species have shown relatively high O<sub>3</sub> tolerance with a damaging threshold of  
462 40 ppbv as calculated with Sitch's scheme (Yue and Unger, 2014). For boreal regions, the  
463 mean [O<sub>3</sub>] of 28 ppbv (Fig. 4a) is much lower than this damaging threshold, explaining why  
464 the excess O<sub>3</sub> stomatal flux (the flux causing damages) is low there (Fig. 8). Statistics in Yue  
465 et al. (2015) show that maximum daily 8-hour average (MDA8) [O<sub>3</sub>] with fire contributions  
466 can be higher than 40 ppbv in Alaska and Canada. However, such episodes appear at 95  
467 percentile for present day and 90 percentile for midcentury, suggesting that O<sub>3</sub> vegetation  
468 damage is rare in boreal North America and fire-induced O<sub>3</sub> enhancement does not  
469 exacerbate such damages. Therefore, we do not consider O<sub>3</sub> damage effects further.

470

471 Fire aerosols cause significant perturbations in shortwave radiation at surface (Fig. 9). The  
472 direct light is largely attenuated especially over Alaska and central Canada, where fire  
473 aerosols are most abundant (Fig. 6). In contrast, diffuse light widely increases due to particle  
474 scattering. In the present day, the average reduction of 5.6 W m<sup>-2</sup> in the direct light  
475 component is in part offset by the enhancement of 2.6 W m<sup>-2</sup> in the diffuse light component,  
476 leading to a net reduction of 3.0 W m<sup>-2</sup> in solar radiation over boreal North America. By the  
477 midcentury, a stronger reduction of 9.5 W m<sup>-2</sup> in direct light is accompanied by an increase of  
478 4.0 W m<sup>-2</sup> in diffuse light, resulting in a net reduction of 5.5 W m<sup>-2</sup> in solar radiation. Fire-  
479 induced BC aerosols strongly absorb solar radiation in the atmospheric column (Figs 10a-  
480 10b). On average, fire aerosols absorb 1.5 W m<sup>-2</sup> in the present day and 2.6 W m<sup>-2</sup> by the  
481 midcentury.

482



483 Atmospheric circulation patterns respond to the aerosol-induced radiative perturbations (Figs  
484 10c-10d). Surface radiative cooling and atmospheric heating together increase air stability  
485 and induce anomalous subsidence. In the present day, such descending motion is confined to  
486 55-68°N, accompanied by a rising motion at 52-55°N (Fig. 10c). As a result, fire aerosols  
487 induce surface warming at higher latitudes but cooling at lower latitudes in boreal regions  
488 (Fig. 11a). Meanwhile, precipitation is inhibited by the subsidence in northwestern Canada  
489 but is promoted by the rising motion in the Southwest (Fig. 11c). By the midcentury, the  
490 range of subsidence expands southward to 42°N (Fig. 10d) due to strengthened atmospheric  
491 heating (Fig. 10b). The downward convection of warm air offsets surface radiative cooling  
492 (Fig. 9b), leading to a significant warming in the Southwest (Fig. 11b). The expanded  
493 subsidence further inhibits precipitation in vast domain of Canada (Fig. 11d). Soil moisture is  
494 closely related to rainfall and as a result exhibits dipole changes (drier north and wetter south)  
495 in the present day (Fig. 11e) but widespread reductions (Fig. 11f) by the midcentury.

496

497 In response to the climatic effects of fire aerosols, boreal NPP shows distinct changes  
498 between the present day and midcentury (Fig. 12). Such changes in NPP are a consequence of  
499 changes in GPP and autotrophic respiration (Fig. S2). Variations in plant respiration resemble  
500 those of GPP, because higher photosynthesis leads to faster leaf/tissue development, resulting  
501 larger maintenance and growth respiration. In the 2010s, forest NPP increases by 5-15% in  
502 Alaska and southern Canada, but decreases by 5-10% in northern and eastern Canada. This  
503 pattern of NPP changes ( $\Delta$ NPP) is connected to the climatic effects of aerosols, especially  
504 changes in soil moisture (Fig. 11). The correlation between  $\Delta$ NPP (Fig. 12a) and changes in  
505 soil moisture (Fig. 11e) reaches  $R = 0.56$  ( $n = 356$ ), much higher than the values of  $R = -0.11$   
506 for temperature change (Fig. 11a) and  $R = 0.22$  for precipitation change (Fig. 11c). At the  
507 continental scale, the patchy responses of NPP offset each other. Since the dominant fraction  
508 of carbon uptake occurs in southern Canada (Fig. 3a), where positive NPP change is  
509 predicted (Fig. 12a), wildfire aerosols enhance the total NPP by  $72 \text{ Tg C yr}^{-1}$  in the present  
510 day (Table 5). In contrast, increased wildfire emissions in the 2050s inhibit precipitation (Fig.  
511 11d) and decrease soil moisture in boreal North America (Fig. 11f), leading to widespread  
512 NPP reductions and a total NPP loss of  $118 \text{ Tg C yr}^{-1}$  (Fig. 12b, Table 5).

513

514

515 **4 Discussion**

516

#### 517 **4.1 Roles of aerosol climatic feedback**

518

519 The contrasting sign of NPP responses in the present day and midcentury are closely related  
520 to the aerosol-induced surface climatic feedback. Sensitivity experiments using offline YIBs  
521 model (Table 3) allowed assessment of the impacts of individual changes in the major  
522 meteorological drivers, including temperature, radiation (diffuse and direct), and soil  
523 moisture (Table 5). The offline simulations driven with changes in all three variables yield  
524  $\Delta\text{NPP}$  of 126 Tg C yr<sup>-1</sup> for the 2010s and -97 Tg C yr<sup>-1</sup> for the 2050s. These values are  
525 different from the online simulations, which predict  $\Delta\text{NPP}$  of 72 Tg C yr<sup>-1</sup> for the 2010s and -  
526 118 Tg C yr<sup>-1</sup> for the 2050s. Missing of other aerosol climatic feedbacks in the offline model,  
527 for example, changes in relative humidity, surface pressure, soil temperature, and turbulence  
528 momentum, may cause such discrepancy between the online and offline simulations.  
529 Seasonal analyses show that summertime  $\Delta\text{NPP}$  is 99 Tg C at present day and -95 Tg C at  
530 midcentury, dominating the NPP changes all through the year, because both wildfire  
531 emissions and ecosystem photosynthesis maximize in boreal summer.

532

533 Observations show that aerosols can promote plant photosynthesis through increasing diffuse  
534 radiation (Niyogi et al., 2004; Cirino et al., 2014; Strada et al., 2015). Our analyses with  
535 ground data also show positive correlations between GPP and PAR<sub>diff</sub> (Fig. 2 and Table 4),  
536 and the model reproduces observed GPP responses to perturbations in direct and diffuse PAR  
537 (Fig. 5). Wildfire aerosols enhance diffuse radiation by 2.6 W m<sup>-2</sup> (1.7%) at present day and  
538 4.0 W m<sup>-2</sup> (2.3%) at midcentury in boreal North America (Fig. 9). With these changes,  
539 simulated NPP increases by 8 Tg C yr<sup>-1</sup> at the 2010s and 14 Tg C yr<sup>-1</sup> at the 2050s (Table 5).  
540 Near the two AmeriFlux sites (Fig. 2a), wildfires increase local AOD by 0.03 (Fig. 6c).  
541 Meanwhile, we estimate that summer average (00:00-24:00) GPP increases by 0.04 μmol m<sup>-2</sup>  
542 s<sup>-1</sup> in the same region due to aerosol diffuse fertilization effects (DFE) based on the results of  
543 (Y10\_PAR – Y10\_CTRL). This change suggests a simulated GPP sensitivity of 1.2 μmol m<sup>-2</sup>  
544 s<sup>-1</sup> (22%) per unit AOD. Observed GPP sensitivity to AOD at the two sites are 2.3 (19%) and  
545 4.5 μmol m<sup>-2</sup> s<sup>-1</sup> (58%) per unit AOD, respectively (Figs 2d-2e). The absolute value of GPP  
546 sensitivity from simulations is much smaller than that of observations, because the former is  
547 for 24-h average while the latter is only for noontime (10:00-14:00). The relative change of  
548 22% in YIBs model falls within the observed range of 19-58%.

549

550 The estimated NPP changes of  $8 \text{ Tg C yr}^{-1}$  by the radiative effects of boreal fire aerosols are  
551 much weaker than the enhancement of  $78\text{-}156 \text{ Tg C yr}^{-1}$  by fires in Amazon basin (Rap et al.,  
552 2015). There are at least two reasons for such a difference in the DFE between boreal and  
553 Amazon fire aerosols. First, wildfire emissions and associated impacts on radiation are much  
554 smaller in boreal regions. Wildfires in Alaska and Canada directly emit  $68 \text{ Tg C yr}^{-1}$  at the  
555 2010s, resulting in enhancement of summer AOD by 35% and diffuse radiation by 1.7%.  
556 These boreal emissions are much smaller than the  $\sim 240 \text{ Tg C yr}^{-1}$  in Amazon basin (van der  
557 Werf et al., 2010), where fires enhances regional PM<sub>2.5</sub> concentrations by 85% and diffuse  
558 radiation by 6.2% in dry seasons (Rap et al., 2015). Second, larger solar insolation in lower  
559 latitudes allows stronger DFE for the same unit change of diffuse radiation. In our prediction,  
560 most of NPP changes occur at high latitudes of boreal regions (Fig. 12), where total  
561 insolation is not so abundant as that at the tropical areas. Consequently, decline of direct  
562 radiation in boreal regions more likely converts the light availability of sunlit leaves from  
563 light-saturation to light-limitation, offsetting the benefit from enhanced diffuse radiation for  
564 shaded leaves. For this study, we do not find GPP reduction by the decline of direct light at  
565 the two Ameriflux sites (Table 4), possibly because these sites are located at middle latitudes  
566 ( $<50^\circ\text{N}$ ). In the future, more observations at higher latitudes ( $> 55^\circ\text{N}$ ) are required to explore  
567 the sensitivity of GPP to AOD at the light-limited conditions.

568

569 Simulations have shown that absorbing aerosols can cause regional drought by increasing air  
570 stability (Liu, 2005; Cook et al., 2009; Tosca et al., 2010). Our results confirm such tendency  
571 but with varied range of hydrological responses depending on the magnitude of wildfire  
572 emissions (Figs 11c-11f). Observations suggest that precipitation (and the associated soil  
573 moisture) is the dominant driver of the changes in GPP over North America, especially for  
574 the domain of cropland (Beer et al., 2010). Sensitivity experiments with offline YIBs model  
575 show that changes in soil moisture account for 82.5% of  $\Delta\text{NPP}$  at present day and 70.5% of  
576  $\Delta\text{NPP}$  at midcentury (Table 5). These results suggest that aerosol-induced changes in soil  
577 water availability, instead of temperature and radiation, dominantly contribute to the changes  
578 of boreal NPP, consistent with observational and experimental results (Ma et al., 2012;  
579 Girardin et al., 2016; Chen et al., 2017).

580

#### 581 **4.2 Limitations and uncertainties**

582

583 In this study, we examine the interactions among climate change, fire activity, air pollution,  
584 and ecosystem productivity. To reduce the complexity of the interactions, we focus on the  
585 most likely dominant feedback and thus main chain of events: “climate → fire → pollution →  
586 biosphere” (Fig. 1). However, our choice of feedback analysis does not mean that the  
587 interplay of other processes is unimportant. For example, climate-induced changes in  
588 vegetation cover/types can influence fire activity by alteration of fuel load, and air pollution  
589 by BVOC emissions (climate → biosphere → fire/pollution). In addition, other feedbacks may  
590 amplify ecosystem responses but are not considered. For example, the drought caused by fire  
591 aerosols in the midcentury (Fig. 11) may help increase fire activity (fire → pollution →  
592 climate → fire). Furthermore, we apply fixed SSTs in the climate simulations because reliable  
593 ocean heat fluxes for the future world were not available. Many previous studies have  
594 investigated regional aerosol-climate feedbacks without ocean responses. For example, Cook  
595 et al. (2009) found that dust-climate-vegetation feedback promotes drought in U.S., with a  
596 climate model driven by prescribed SSTs. Similarly, Liu (2005) found fire aerosols enhance  
597 regional drought using a regional climate model, which even ignores the feedback between  
598 local climate and large-scale circulation. While we do concede that our experimental design  
599 is not a complete assessment of all known processes and feedbacks, within these limitations,  
600 this study for the first time quantifies the indirect impacts of wildfire on long-range  
601 ecosystem productivity under climate change.

602

603 We use the ensemble projected fire emissions from Yue et al. (2015). Area burned is  
604 predicted based on the simulated meteorology from multiple climate models. Such an  
605 approach may help reduce model uncertainties in climatic responses to CO<sub>2</sub> changes (Collins  
606 et al., 2013; Kirtman et al., 2014), but cannot remove the possible biases in the selection of  
607 climate scenarios and fire models. All predictions in Yue et al. (2015) are performed under  
608 the IPCC A1B scenario. With two different scenarios, A2 of high emissions and B2 of low  
609 emissions, Balshi et al. (2009) showed that future area burned in boreal North America  
610 increases at a similar rate until the 2050s, after which area burned in A2 scenario increases  
611 much faster than that in B2 scenario. On average, boreal area burned in Balshi et al. (2009)  
612 increases by ~160% at 2051-2060 compared with 2001-2010, much higher than the change of  
613 66% in Yue et al. (2015). In contrast, Amiro et al. (2009) predicted that boreal area burned at  
614 the 2×CO<sub>2</sub> scenario increases only by 34% relative to the 1×CO<sub>2</sub> scenario. This ratio is only

615 half of the estimate in Yue et al. (2015), which compared results between periods with  
616  $1.44\times\text{CO}_2$  and  $1\times\text{CO}_2$ . The discrepancies among these studies are more likely attributed to  
617 the differences in fire models. Although both Amiro et al. (2009) and Yue et al. (2015)  
618 developed fire-weather regressions in boreal ecoregions, the former study did not include  
619 geopotential height at 500 hPa and surface relative humidity as predictors, which make  
620 dominant contributions to area burned changes in the latter study. On the other hand, Balshi  
621 et al. (2009) developed nonlinear regressions between area burned and climate at grid scale,  
622 which helps retain extreme values at both the temporal and spatial domain. Compared to  
623 previous estimates, Yue et al. (2015) predicted median increases in future fire emissions over  
624 boreal North America.

625

626 We apply constant land cover and fuel load for both present day and midcentury, but we  
627 estimate an increase in fuel consumption due to changes in fuel moisture. Future projection of  
628 boreal fuel load is highly uncertain because of multiple contrasting influences. For example,  
629 using a dynamic global vegetation model (DGVM) and an ensemble of climate change  
630 projections, Heyder et al. (2011) predicted a large-scale dieback in boreal-temperate forests  
631 due to increased heat and drought stress in the coming decades. On the contrary, projections  
632 using DGVMs show a widespread increase in vegetation carbon under the global warming  
633 scenario with  $\text{CO}_2$  fertilization of photosynthesis (Friend et al., 2014; Knorr et al., 2016). In  
634 addition, compound factors such as greenhouse gas mitigation (Kim et al., 2017), population  
635 change (Knorr et al., 2016), pine beetle outbreak (Kurz et al., 2008), and fire management  
636 (Doerr and Santin, 2016) may exert varied impacts on future vegetation and fuel load.  
637 Although we apply constant fuel load, we consider changes of fuel moisture because warmer  
638 climate states tend to dry fuel and increase fuel consumption (Flannigan et al., 2016). With  
639 constant fuel load but climate-driven fuel moisture, we calculate a 9% increase in boreal fuel  
640 consumption by the midcentury (Yue et al., 2015). Although such increment is higher than  
641 the prediction of 2-5% by Amiro et al. (2009) for a doubled- $\text{CO}_2$  climate, the consumption-  
642 induced uncertainty for fire emission is likely limited because changes in area burned are  
643 much more profound.

644

645 Predicted surface  $[\text{O}_3]$  is much higher than observations over boreal North America (Fig. 4).  
646 This bias does not affect main conclusions of this study, because predicted  $\text{O}_3$  causes limited  
647 damages to boreal GPP even with the overestimated  $[\text{O}_3]$  (Fig. 7). The result confirms that

Xu Yue 10/11/17 11:07 PM

Deleted: multiple

Xu Yue 10/11/17 11:07 PM

Deleted: boreal

Xu Yue 10/11/17 11:07 PM

Deleted: (Friend et al., 2014).

Xu Yue 10/11/17 11:07 PM

Deleted: pine beetle outbreak (Kurz et al., 2008)

653 fire-induced O<sub>3</sub> vegetation damage is negligible in boreal North America. For aerosols, the  
654 model captures reasonable spatial pattern of AOD but with a background value of ~0.1  
655 outside fire-prone regions, where the observed AOD is usually 0.1-0.2 (Fig. 3). This  
656 discrepancy may be related to the insufficient representations of physical and chemical  
657 processes in the model, but may also result from the retrieval biases in MODIS data due to  
658 the poor surface conditions (Liu et al., 2005) and small AOD variations (Vachon et al., 2004)  
659 at high latitudes.

660

661 Simulated aerosol climatic effects depend on radiative and physical processes implemented in  
662 the climate model. We find that present-day boreal fire aerosols on average absorb  $1.5 \text{ W m}^{-2}$   
663 in the atmosphere (Fig. 10), which is much smaller than the value of  $20.5 \pm 9.3 \text{ W m}^{-2}$  for  
664 fires in equatorial Asia (Tosca et al., 2010). This is because boreal fires enhance AOD only  
665 by 0.03 while tropical fires increase AOD by ~0.4. Previous modeling studies showed that  
666 fire plumes induce regional and downwind drought through enhanced atmospheric stability  
667 (Feingold et al., 2005; Tosca et al., 2010; Liu et al., 2014). Most of these results were based  
668 on the direct and/or semi-direct radiative effects of fire aerosols. Inclusion of the indirect  
669 aerosol effect may further inhibit precipitation and amplify drought, but may also introduce  
670 additional uncertainties for the simulations. The fire-drought interaction may promote fire  
671 activity, especially in a warmer climate. Ignoring this interaction may underestimate future  
672 area burned and the consequent emissions.

673

#### 674 **4.3 Implications**

675

676 Inverse modeling studies have shown that the land ecosystems of boreal North America are  
677 carbon neutral in the present day, with the estimated land-to-air carbon flux from  $-270 \pm 130$   
678  $\text{Tg C yr}^{-1}$  to  $300 \pm 500 \text{ Tg C yr}^{-1}$  (Gurney et al., 2002; Rodenbeck et al., 2003; Baker et al.,  
679 2006; Jacobson et al., 2007; Deng et al., 2014). Here, we reveal a missing land carbon source  
680 due to future wildfire pollution, taking into account full coupling among fire activity, climate  
681 change, air pollution, and the carbon cycle. Fire pollution aerosol increases boreal NPP by 72  
682  $\text{Tg C yr}^{-1}$  in the present day, comparable to the direct carbon loss of  $68 \text{ Tg C yr}^{-1}$  from  
683 wildfire CO<sub>2</sub> emissions (product of biomass burned and CO<sub>2</sub> emission factors). By  
684 midcentury, increasing fire emissions instead cause a NPP reduction of  $118 \text{ Tg C yr}^{-1}$  due to  
685 the amplified drought. Although NPP is not a direct indicator of the land carbon sink,

686 reduction of NPP is always accompanied with the decline of net ecosystem exchange (NEE)  
687 and the enhanced carbon loss. In combination with the enhanced carbon emission of 130 Tg  
688 C yr<sup>-1</sup>, future boreal wildfire presents an increasing threat to the regional carbon balance and  
689 global warming mitigation. Furthermore, the NPP reductions are mostly located in southern  
690 Canada, where cropland is the dominant ecosystem, newly exposing the future wildfire-  
691 related air pollution risk to food production.

692

693 Our analyses of fire pollution effects on boreal North American productivity may not be  
694 representative for other boreal ecosystems and/or on the global scale. There is substantial  
695 variability in plant species, topography, and climatology across different boreal regions. Such  
696 differences indicate distinct GPP sensitivities as well as fire characteristics. At lower latitudes,  
697 where anthropogenic pollution emissions are more abundant, ambient ozone concentrations  
698 may have exceeded damaging thresholds for most plant species. In those regions, additional  
699 ozone from a fire plume may cause more profound impacts on photosynthesis than our  
700 estimate for boreal North America. For example, Amazonian fire is predicted to reduce forest  
701 NPP by 230 Tg C yr<sup>-1</sup> through the generation of surface ozone (Pacífico et al., 2015).  
702 Meanwhile, solar radiation is more abundant at lower latitudes, indicating more efficient  
703 increases in photosynthesis through aerosol DFE because the sunlit leaves receive saturated  
704 direct light in those regions. As shown in Beer et al. (2010), partial correlations between GPP  
705 and solar radiation are positive in boreal regions but negative over the subtropics/tropics,  
706 suggesting that light extinction by fire aerosols has contrasting impacts on plant  
707 photosynthesis in the high versus low latitudes. Further simulations and analyses are required  
708 to understand the net impacts of ozone and aerosols from biomass burning on the global  
709 carbon cycle.

710

711

712 *Acknowledgements.* Xu Yue acknowledges funding support from the National Key Research  
713 and Development Program of China (Grant No. 2017YFA0603802), the National Basic  
714 Research Program of China (973 program, Grant No. 2014CB441202) and the “Thousand  
715 Youth Talents Plan”. Nadine Unger acknowledges funding support from The University of  
716 Exeter.

717

718  
719  
720  
721

**Table 1.** Online simulations with ModelE2-YIBs climate model <sup>a</sup>

Simulations	SST	[CO <sub>2</sub> ]	Emissions	Fires	O <sub>3</sub> effect	Aerosol effect
F10O3	2010s	2010s	2010s	2010s	Yes	No
F10AERO	2010s	2010s	2010s	2010s	No	Yes
F10CTRL	2010s	2010s	2010s	No	No	Yes
F50O3	2050s	2050s	2050s	2050s	Yes	No
F50AERO	2050s	2050s	2050s	2050s	No	Yes
F50CTRL	2050s	2050s	2050s	No	No	Yes

722  
723  
724  
725  
726  
727  
728

<sup>a</sup> Values of SST, [CO<sub>2</sub>], and emissions are adopted from RCP8.5 scenario, with the average of 2006-2015 for the 2010s and that of 2046-2055 for the 2050s. For fire emissions, values at the 2010s are predicted based on meteorology for 1981-2000 and those at the 2050s are for 2046-2065.



729  
730  
731  
732

**Table 2.** Emissions from wildfires and non-fire sources over boreal North America

Species	Fire emissions (Tg yr <sup>-1</sup> )		Non-fire emissions (Tg yr <sup>-1</sup> )	
	2010s	2050s	2010s	2050s
NO <sub>x</sub> <sup>a</sup>	0.39	0.74	2.43	2.08
CO	15.7	28.8	5.9	4.0
SO <sub>2</sub> <sup>a</sup>	0.12	0.22	1.95	1.28
NH <sub>3</sub>	0.22	0.40	0.80	1.15
BC	0.08	0.16	0.03	0.01
OC	1.10	2.04	0.04	0.02
NMVOC	0.39	1.34	0.49	0.30
BVOC <sup>b</sup>	N/A	N/A	15.3	15.1

733  
734  
735  
736  
737  
738

<sup>a</sup> Natural emissions are included for NO<sub>x</sub> (lightning and soil) and SO<sub>2</sub> (volcano).

<sup>b</sup> ModelE2-YIBs calculates BVOC emissions using photosynthesis-dependent scheme implemented by Unger et al. (2013).

739  
740  
741  
742  
743  
744

**Table 3.** Simulations with YIBs vegetation model driven by offline meteorology from ModelE2-YIBs climate model

Simulations	Base forcing	Temperature	PAR	Soil moisture
Y10_CTRL	F10CTRL			
Y10_ALL	F10CTRL	F10AERO	F10AERO	F10AERO
Y10_TAS	F10CTRL	F10AERO		
Y10_PAR	F10CTRL		F10AERO	
Y10_SLM	F10CTRL			F10AERO
Y50_CTRL	F50CTRL			
Y50_ALL	F50CTRL	F50AERO	F50AERO	F50AERO
Y50_TAS	F50CTRL	F50AERO		
Y50_PAR	F50CTRL		F50AERO	
Y50_SLM	F50CTRL			F50AERO

745  
746  
747  
748  
749

750  
751 **Table 4.** Pearson's correlation coefficients for GPP-PAR and GPP-AOD relationships at  
752 Ameriflux (AMF) sites <sup>a</sup>  
753  
754

Site	Period <sup>b</sup>	Pearson's <i>R</i>					
		GPP-PAR	GPP-PAR <sub>dir</sub>	GPP-PAR <sub>dif</sub>	GPP-AOD	AOD-PAR <sub>dif</sub>	AOD-PAR <sub>dir</sub>
CA-Gro	2004-2013	<b>0.19</b> (2432)	-0.01 (2432)	<b>0.42</b> (2432)	0.15 (65)	<b>0.60</b> (65)	<b>-0.52</b> (65)
CA-Qfo	2003-2014	<b>0.16</b> (3201)	<b>-0.04</b> (3201)	<b>0.45</b> (3201)	<b>0.36</b> (59)	<b>0.91</b> (34)	<b>-0.80</b> (34)

755  
756 <sup>a</sup> Both GPP and PAR (direct PAR<sub>dir</sub> and diffuse PAR<sub>dif</sub>) data are adopted from site-level AMF  
757 measurements. AOD data are adopted from instantaneous MODIS Aqua and Terra 3-km  
758 retrievals. Correlations are calculated for quasi-coincident AMF and MODIS data over  
759 summer noontime (June-August, 10:00-14:00 Local Time). The sampling number for each  
760 correlation is denoted in brackets. Significant ( $p < 0.05$ ) correlation coefficients are bolded.  
761 <sup>b</sup> For CA-Gro site, diffuse PAR observations of 2005-2009 have been discarded because of  
762 poor calibration, as documented on the AMF website.  
763  
764

765  
766  
767  
768  
769  
770

**Table 5.** Changes in NPP ( $\text{Tg C yr}^{-1}$ ) caused by composite and individual climatic effects of fire aerosols

	2010s	2050s
Online <sup>a</sup>	72	-118
Offline total <sup>b</sup>	126	-97
Temperature	11	-22
Radiation	8	14
Soil moisture	104	-86

771  
772 <sup>a</sup> Online results are calculated using the ModelE2-YIBs model with (F10AERO – F10CTRL)  
773 for the 2010s and (F50AERO – F50CTRL) for the 2050s.

774 <sup>b</sup> Offline results are calculated with the YIBs model driven with individual or combined  
775 changes in temperature, radiation, and soil moisture.

776  
777  
778  
779  
780  
781  
782  
783

784 **References**

- 785 Alvarado, M. J., Logan, J. A., Mao, J., Apel, E., Riemer, D., Blake, D., Cohen, R. C., Min, K.  
786 E., Perring, A. E., Browne, E. C., Wooldridge, P. J., Diskin, G. S., Sachse, G. W.,  
787 Fuelberg, H., Sessions, W. R., Harrigan, D. L., Huey, G., Liao, J., Case-Hanks, A.,  
788 Jimenez, J. L., Cubison, M. J., Vay, S. A., Weinheimer, A. J., Knapp, D. J., Montzka, D.  
789 D., Flocke, F. M., Pollack, I. B., Wennberg, P. O., Kurten, A., Crouse, J., St Clair, J. M.,  
790 Wisthaler, A., Mikoviny, T., Yantosca, R. M., Carouge, C. C., and Le Sager, P.:  
791 Nitrogen oxides and PAN in plumes from boreal fires during ARCTAS-B and their  
792 impact on ozone: an integrated analysis of aircraft and satellite observations, *Atmos.*  
793 *Chem. Phys.*, 10, 9739-9760, doi:10.5194/Acp-10-9739-2010, 2010.
- 794 Amiro, B. D., Cantin, A., Flannigan, M. D., and de Groot, W. J.: Future emissions from  
795 Canadian boreal forest fires, *Can. J. For. Res.*, 39, 383-395, doi:10.1139/X08-154, 2009.
- 796 Andreae, M. O., and Merlet, P.: Emission of trace gases and aerosols from biomass burning,  
797 *Global Biogeochemical Cycles*, 15, 955-966, 2001.
- 798 Atkin, O. K., and Tjoelker, M. G.: Thermal acclimation and the dynamic response of plant  
799 respiration to temperature, *Trends in Plant Science*, 8, 343-351, doi:10.1016/S1360-  
800 1385(03)00136-5, 2003.
- 801 Baker, D. F., Law, R. M., Gurney, K. R., Rayner, P., Peylin, P., Denning, A. S., Bousquet, P.,  
802 Bruhwiler, L., Chen, Y. H., Ciais, P., Fung, I. Y., Heimann, M., John, J., Maki, T.,  
803 Maksyutov, S., Masarie, K., Prather, M., Pak, B., Taguchi, S., and Zhu, Z.: TransCom 3  
804 inversion intercomparison: Impact of transport model errors on the interannual  
805 variability of regional CO<sub>2</sub> fluxes, 1988-2003, *Global Biogeochemical Cycles*, 20,  
806 Gb1002, doi:10.1029/2004gb002439, 2006.
- 807 Ball, J. T., Woodrow, I. E., and Berry, J. A.: A model predicting stomatal conductance and its  
808 contribution to the control of photosynthesis under different environmental conditions,  
809 in: *Progress in Photosynthesis Research*, edited by: Biggins, J., Nijhoff, Dordrecht,  
810 Netherlands, 110–112, 1987.
- 811 Balshi, M. S., McGuirez, A. D., Duffy, P., Flannigan, M., Walsh, J., and Melillo, J.:  
812 Assessing the response of area burned to changing climate in western boreal North  
813 America using a Multivariate Adaptive Regression Splines (MARS) approach, *Global*  
814 *Change Biology*, 15, 578-600, doi:10.1111/J.1365-2486.2008.01679.X, 2009.
- 815 Beer, C., Reichstein, M., Tomelleri, E., Ciais, P., Jung, M., Carvalhais, N., Rodenbeck, C.,  
816 Arain, M. A., Baldocchi, D., Bonan, G. B., Bondeau, A., Cescatti, A., Lasslop, G.,  
817 Lindroth, A., Lomas, M., Luyssaert, S., Margolis, H., Oleson, K. W., Rouspard, O.,  
818 Veenendaal, E., Viovy, N., Williams, C., Woodward, F. I., and Papale, D.: Terrestrial  
819 Gross Carbon Dioxide Uptake: Global Distribution and Covariation with Climate,  
820 *Science*, 329, 834-838, doi:10.1126/Science.1184984, 2010.
- 821 Bergeron, Y., Cyr, D., Girardin, M. P., and Carcaillet, C.: Will climate change drive 21st  
822 century burn rates in Canadian boreal forest outside of its natural variability: collating  
823 global climate model experiments with sedimentary charcoal data, *International Journal*  
824 *of Wildland Fire*, 19, 1127-1139, doi:10.1071/Wf09092, 2010.

825 Bond-Lamberty, B., Peckham, S. D., Ahl, D. E., and Gower, S. T.: Fire as the dominant  
826 driver of central Canadian boreal forest carbon balance, *Nature*, 450, 89-92,  
827 doi:10.1038/Nature06272, 2007.

828 Chen, L., Huang, J.-G., Alam, S. A., Zhai, L., Dawson, A., Stadt, K. J., and Comeau, P. G.:  
829 Drought causes reduced growth of trembling aspen in western Canada, *Global Change*  
830 *Biology*, in press, doi:10.1111/gcb.13595, 2017.

831 Cirino, G. G., Souza, R. A. F., Adams, D. K., and Artaxo, P.: The effect of atmospheric  
832 aerosol particles and clouds on net ecosystem exchange in the Amazon, *Atmospheric*  
833 *Chemistry and Physics*, 14, 6523-6543, doi:10.5194/acp-14-6523-2014, 2014.

834 Cohan, D. S., Xu, J., Greenwald, R., Bergin, M. H., and Chameides, W. L.: Impact of  
835 atmospheric aerosol light scattering and absorption on terrestrial net primary productivity,  
836 *Global Biogeochemical Cycles*, 16, 1090, doi:10.1029/2001gb001441, 2002.

837 Collins, M., Knutti, R., Arblaster, J., Dufresne, J.-L., Fichet, T., Friedlingstein, P., Gao, X.,  
838 Jr., W. J. G., Johns, T., Krinner, G., Shongwe, M., Tebaldi, C., Weaver, A. J., and  
839 Wehner, M.: Long-term Climate Change: Projections, Commitments and Irreversibility,  
840 in: *Climate Change 2013: The Physical Science Basis. Contribution of Working Group I*  
841 *to the Fifth Assessment Report of the Intergovernmental Panel on Climate Change*,  
842 edited by: Stocker, T. F., Qin, D., Plattner, G.-K., Tignor, M., Allen, S. K., Boschung, J.,  
843 Nauels, A., Xia, Y., Bex, V., and Midgley, P. M., Cambridge University Press,  
844 Cambridge, United Kingdom and New York, NY, USA., 1029-1136, 2013.

845 Cook, B. I., Miller, R. L., and Seager, R.: Amplification of the North American "Dust Bowl"  
846 drought through human-induced land degradation, *Proceedings of the National Academy*  
847 *of Sciences of the United States of America*, 106, 4997-5001,  
848 doi:10.1073/pnas.0810200106, 2009.

849 Cox, P. M.: Description of the "TRIFFID" Dynamic Global Vegetation Model, Hadley  
850 Centre technical note 24, 2001.

851 de Groot, W. J., Flannigan, M. D., and Cantin, A. S.: Climate change impacts on future  
852 boreal fire regimes, *Forest Ecology and Management*, 294, 35-44,  
853 doi:10.1016/j.foreco.2012.09.027, 2013.

854 Deng, F., Jones, D. B. A., Henze, D. K., Bousseres, N., Bowman, K. W., Fisher, J. B., Nassar,  
855 R., O'Dell, C., Wunch, D., Wennberg, P. O., Kort, E. A., Wofsy, S. C., Blumenstock, T.,  
856 Deutscher, N. M., Griffith, D. W. T., Hase, F., Heikkinen, P., Sherlock, V., Strong, K.,  
857 Sussmann, R., and Warneke, T.: Inferring regional sources and sinks of atmospheric  
858 CO<sub>2</sub> from GOSAT XCO<sub>2</sub> data, *Atmospheric Chemistry and Physics*, 14, 3703-3727,  
859 doi:10.5194/acp-14-3703-2014, 2014.

860 Doerr, S. H., and Santin, C.: Global trends in wildfire and its impacts: perceptions versus  
861 realities in a changing world, *Phil. Trans. R. Soc. B*, 371, doi:10.1098/rstb.2015.0345,  
862 2016.

863 Duffy, P. A., Walsh, J. E., Graham, J. M., Mann, D. H., and Rupp, T. S.: Impacts of large-  
864 scale atmospheric-ocean variability on Alaskan fire season severity, *Ecological*  
865 *Applications*, 15, 1317-1330, doi:Doi 10.1890/04-0739, 2005.

866 Farquhar, G. D., Caemmerer, S. V., and Berry, J. A.: A Biochemical-Model of  
867 Photosynthetic Co<sub>2</sub> Assimilation in Leaves of C-3 Species, *Planta*, 149, 78-90,  
868 doi:10.1007/Bf00386231, 1980.

869 Feingold, G., Jiang, H., and Harrington, J. Y.: On smoke suppression of clouds in Amazonia,  
870 *Geophysical Research Letters*, 32, L02804, doi:10.1029/2004GL021369, 2005.

871 Flannigan, M. D., Logan, K. A., Amiro, B. D., Skinner, W. R., and Stocks, B. J.: Future area  
872 burned in Canada, *Clim. Change*, 72, 1-16, doi:10.1007/S10584-005-5935-Y, 2005.

873 Flannigan, M. D., Wotton, B. M., Marshall, G. A., Groot, W. J. d., Johnston, J., Jurko, N.,  
874 and Cantin, A. S.: Fuel moisture sensitivity to temperature and precipitation: climate  
875 change implications, *Climatic Change*, 134, 59, doi:10.1007/s10584-015-1521-0, 2016.

876 Flato, G., Marotzke, J., Abiodun, B., Braconnot, P., Chou, S. C., Collins, W., Cox, P.,  
877 Driouech, F., Emori, S., Eyring, V., Forest, C., Gleckler, P., Guilyardi, E., Jakob, C.,  
878 Kattsov, V., Reason, C., and Rummukainen, M.: Evaluation of Climate Models, in:  
879 *Climate Change 2013: The Physical Science Basis. Contribution of Working Group I to*  
880 *the Fifth Assessment Report of the Intergovernmental Panel on Climate Change*, edited  
881 by: Stocker, T. F., Qin, D., Plattner, G.-K., Tignor, M., Allen, S. K., Boschung, J.,  
882 Nauels, A., Xia, Y., Bex, V., and Midgley, P. M., Cambridge University Press,  
883 Cambridge, United Kingdom and New York, NY, USA, 465-570, 2013.

884 Friend, A. D., Lucht, W., Rademacher, T. T., Keribin, R., Betts, R., Cadule, P., Ciais, P.,  
885 Clark, D. B., Dankers, R., Falloon, P. D., Ito, A., Kahana, R., Kleidon, A., Lomas, M. R.,  
886 Nishina, K., Ostberg, S., Pavlick, R., Peylin, P., Schaphoff, S., Vuichard, N.,  
887 Warszawski, L., Wiltshire, A., and Woodward, F. I.: Carbon residence time dominates  
888 uncertainty in terrestrial vegetation responses to future climate and atmospheric CO<sub>2</sub>,  
889 *Proc. Natl. Acad. Sci. u. s. a.*, 111, 3280-3285, doi:10.1073/pnas.1222477110, 2014.

890 Gillett, N. P., Weaver, A. J., Zwiers, F. W., and Flannigan, M. D.: Detecting the effect of  
891 climate change on Canadian forest fires, *Geophys. Res. Lett.*, 31, L18211,  
892 doi:10.1029/2004gl020876, 2004.

893 Girardin, M. P., and Mudelsee, M.: Past and future changes in Canadian boreal wildfire  
894 activity, *Ecological Applications*, 18, 391-406, doi:Doi 10.1890/07-0747.1, 2008.

895 Girardin, M. P., Hogg, E. H., Bernier, P. Y., Kurz, W. A., Guo, X. J., and Cyr, G.: Negative  
896 impacts of high temperatures on growth of black spruce forests intensify with the  
897 anticipated climate warming, *Global Change Biology*, 22, 627-643,  
898 doi:10.1111/gcb.13072, 2016.

899 Groot, W. J. d., D.Flannigan, M., and S.Cantin, A.: Climate change impacts on future boreal  
900 fire regimes, *Forest Ecology and Management*, 294, doi:10.1016/j.foreco.2012.09.027,  
901 2013.

902 Gurney, K. R., Law, R. M., Denning, A. S., Rayner, P. J., Baker, D., Bousquet, P., Bruhwiler,  
903 L., Chen, Y. H., Ciais, P., Fan, S., Fung, I. Y., Gloor, M., Heimann, M., Higuruchi, K.,  
904 John, J., Maki, T., Maksyutov, S., Masarie, K., Peylin, P., Prather, M., Pak, B. C.,  
905 Randerson, J., Sarmiento, J., Taguchi, S., Takahashi, T., and Yuen, C. W.: Towards  
906 robust regional estimates of CO<sub>2</sub> sources and sinks using atmospheric transport models,  
907 *Nature*, 415, 626-630, doi:10.1038/415626a, 2002.

908 Hansen, M. C., DeFries, R. S., Townshend, J. R. G., Carroll, M., Dimiceli, C., and Sohlberg,  
909 R. A.: Global Percent Tree Cover at a Spatial Resolution of 500 Meters: First Results of  
910 the MODIS Vegetation Continuous Fields Algorithm, *Earth Interactions*, 7, 1-15,  
911 doi:10.1175/1087-3562(2003)007<0001:GPTCAA>2.0.CO;2, 2003.

912 Heyder, U., Schaphoff, S., Gerten, D., and Lucht, W.: Risk of severe climate change impact  
913 on the terrestrial biosphere, *Environmental Research Letters*, 6, 034036,  
914 doi:10.1088/1748-9326/6/3/034036, 2011.

915 Jacobson, A. R., Fletcher, S. E. M., Gruber, N., Sarmiento, J. L., and Gloor, M.: A joint  
916 atmosphere-ocean inversion for surface fluxes of carbon dioxide: 2. Regional results,  
917 *Global Biogeochemical Cycles*, 21, Gb1020, doi:10.1029/2006gb002703, 2007.

918 Jung, M., Reichstein, M., and Bondeau, A.: Towards global empirical upscaling of  
919 FLUXNET eddy covariance observations: validation of a model tree ensemble approach  
920 using a biosphere model, *Biogeosciences*, 6, 2001-2013, doi:10.5194/bg-6-2001-2009,  
921 2009.

922 Kanniah, K. D., Beringer, J., North, P., and Hutley, L.: Control of atmospheric particles on  
923 diffuse radiation and terrestrial plant productivity: A review, *Progress in Physical  
924 Geography*, 36, 209-237, doi:10.1177/0309133311434244, 2012.

925 Kasischke, E. S., and Turetsky, M. R.: Recent changes in the fire regime across the North  
926 American boreal region - Spatial and temporal patterns of burning across Canada and  
927 Alaska, *Geophys. Res. Lett.*, 33, doi:10.1029/2006gl025677, 2006.

928 Keane, R. E., Agee, J. K., Fule, P., Keeley, J. E., Key, C., Kitchen, S. G., Miller, R., and  
929 Schulte, L. A.: Ecological effects of large fires on US landscapes: benefit or catastrophe?,  
930 *International Journal of Wildland Fire*, 17, 696-712, doi:10.1071/Wf07148, 2008.

931 Kim, J. B., Monier, E., Sohngen, B., Pitts, G. S., Drapek, R., McFarland, J., Ohrel, S., and  
932 Cole, J.: Assessing climate change impacts, benefits of mitigation, and uncertainties on  
933 major global forest regions under multiple socioeconomic and emissions scenarios,  
934 *Environmental Research Letters*, 12, 045001, doi:10.1088/1748-9326/aa63fc, 2017.

935 Kirtman, B. P., Min, D., Infanti, J. M., Kinter, J. L., III, Paolino, D. A., Zhang, Q., van den  
936 Dool, H., Saha, S., Mendez, M. P., Becker, E., Peng, P., Tripp, P., Huang, J., DeWitt, D.  
937 G., Tippett, M. K., Barnston, A. G., Li, S., Rosati, A., Schubert, S. D., Rienecker, M.,  
938 Suarez, M., Li, Z. E., Marshak, J., Lim, Y.-K., Tribbia, J., Pegion, K., Merryfield, W. J.,  
939 Denis, B., and Wood, E. F.: The North American Multimodel Ensemble: Phase-1  
940 Seasonal-to-Interannual Prediction; Phase-2 toward Developing Intraseasonal Prediction,  
941 *Bulletin of the American Meteorological Society*, 95, 585-601, 2014.

942 [Knorr, W., Jiang, L., and Arneth, A.: Climate, CO2 and human population impacts on global  
943 wildfire emissions, \*Biogeosciences\*, 13, 267-282, doi:10.5194/bg-13-267-2016, 2016.](#)

944 Kurz, W. A., Dymond, C. C., Stinson, G., Rampley, G. J., Neilson, E. T., Carroll, A. L.,  
945 Ebata, T., and Safranyik, L.: Mountain pine beetle and forest carbon feedback to climate  
946 change, *Nature*, 452, 987-990, doi:10.1038/nature06777, 2008.

947 Levy, R. C., Mattoo, S., Munchak, L. A., Remer, L. A., Sayer, A. M., Patadia, F., and Hsu, N.  
948 C.: The Collection 6 MODIS aerosol products over land and ocean, *Atmospheric  
949 Measurement Techniques*, 6, 2989-3034, doi:10.5194/amt-6-2989-2013, 2013.



950 Liu, H. Q., Pinker, R. T., and Holben, B. N.: A global view of aerosols from merged transport  
951 models, satellite, and ground observations, *J. Geophys. Res.*, 110, -, 2005.

952 Liu, J. C., Wilson, A., Mickley, L. J., Ebisu, K., Wang, Y., Sulprizio, M. P., Peng, R. D., Yue,  
953 X., Son, J.-Y., Anderson, G. B., Dominici, F., and Bell, M. L.: Wildfire-specific Fine  
954 Particulate Matter and Risk of Hospital Admissions in Urban and Rural Counties,  
955 *Epidemiology*, 28, 77-85, doi:10.1097/EDE.0000000000000556, 2017.

956 Liu, Y.: Enhancement of the 1988 northern U.S. drought due to wildfires, *Geophysical  
957 Research Letters*, 32, L10806, doi:10.1029/2005GL022411, 2005.

958 Liu, Y., Goodrick, S., and Heilman, W.: Wildland fire emissions, carbon, and climate:  
959 Wildfire–climate interactions, *Forest Ecology and Management*, 317, 80-96,  
960 doi:10.1016/j.foreco.2013.02.020, 2014.

961 Ma, Z. H., Peng, C. H., Zhu, Q. A., Chen, H., Yu, G. R., Li, W. Z., Zhou, X. L., Wang, W. F.,  
962 and Zhang, W. H.: Regional drought-induced reduction in the biomass carbon sink of  
963 Canada's boreal forests, *Proceedings of the National Academy of Sciences of the United  
964 States of America*, 109, 2423-2427, doi:10.1073/pnas.1111576109, 2012.

965 McKenzie, D., Raymond, C. L., Kellogg, L. K. B., Norheim, R. A., Andreu, A. G., Bayard, A.  
966 C., Kopper, K. E., and Elman, E.: Mapping fuels at multiple scales: landscape  
967 application of the Fuel Characteristic Classification System, *Can. J. For. Res.*, 37, 2421-  
968 2437, doi:10.1139/X07-056, 2007.

969 Meehl, G. A., Covey, C., Delworth, T., Latif, M., McAvaney, B., Mitchell, J. F. B., Stouffer,  
970 R. J., and Taylor, K. E.: The WCRP CMIP3 multi-model dataset: A new era in climate  
971 change research, *Bull. Am. Meteorol. Soc.*, 88, 1383-1394, doi:10.1175/BAMS-88-9-  
972 1383, 2007.

973 Mercado, L. M., Bellouin, N., Sitch, S., Boucher, O., Huntingford, C., Wild, M., and Cox, P.  
974 M.: Impact of changes in diffuse radiation on the global land carbon sink, *Nature*, 458,  
975 1014-1017, doi:10.1038/Nature07949, 2009.

976 Moritz, M. A., Parisien, M.-A., Battlori, E., Krawchuk, M. A., Dorn, J. V., Ganz, D. J., and  
977 Hayhoe, K.: Climate change and disruptions to global fire activity, *Ecosphere*, 3,  
978 doi:10.1890/ES11-00345.1, 2012.

979 Morris, G. A., Hersey, S., Thompson, A. M., Pawson, S., Nielsen, J. E., Colarco, P. R.,  
980 McMillan, W. W., Stohl, A., Turquety, S., Warner, J., Johnson, B. J., Kucsera, T. L.,  
981 Larko, D. E., Oltmans, S. J., and Witte, J. C.: Alaskan and Canadian forest fires  
982 exacerbate ozone pollution over Houston, Texas, on 19 and 20 July 2004, *Journal of  
983 Geophysical Research-Atmospheres*, 111, D24s03, doi:10.1029/2006jd007090, 2006.

984 Munchak, L. A., Levy, R. C., Mattoo, S., Remer, L. A., Holben, B. N., Schafer, J. S.,  
985 Hostetler, C. A., and Ferrare, R. A.: MODIS 3 km aerosol product: applications over  
986 land in an urban/suburban region, *Atmospheric Measurement Techniques*, 6, 1747-1759,  
987 doi:10.5194/amt-6-1747-2013, 2013.

988 Nadeau, L. B., McRae, D. J., and Jin, J. Z.: Development of a national fuel-type map for  
989 Canada using fuzzy logic, Natural Resources Canada, Canadian Forest Service, Northern  
990 Forestry Centre, Edmonton, Alberta. Information Report NOR-X-406, 2005.

991 Nitschke, C. R., and Innes, J. L.: Climatic change and fire potential in South-Central British  
992 Columbia, Canada, *Global Change Biology*, 14, 841-855, doi:10.1111/j.1365-  
993 2486.2007.01517.x, 2008.

994 Niyogi, D., Chang, H.-I., Saxena, V. K., Holt, T., Alapaty, K., Booker, F., Chen, F., Davis, K.  
995 J., Holben, B., Matsui, T., Meyers, T., Oechel, W. C., Sr., R. A. P., Wells, R., Wilson, K.,  
996 and Xue, Y.: Direct observations of the effects of aerosol loading on net ecosystem CO<sub>2</sub>  
997 exchanges over different landscapes, *Geophysical Research Letters*, 31,  
998 doi:10.1029/2004GL020915, 2004.

999 Oleson, K. W., Lawrence, D. M., Bonan, G. B., Flanne, M. G., Kluzek, E., Lawrence, P. J.,  
1000 Levis, S., Swenson, S. C., and Thornton, P. E.: Technical Description of version 4.0 of  
1001 the Community Land Model (CLM), National Center for Atmospheric Research,  
1002 Boulder, CONCAR/TN-478+STR, 2010.

1003 Oliveira, P. H. F., Artaxo, P., Pires, C., de Lucca, S., Procópio, A., Holben, B., Schafer, J.,  
1004 Cardoso, L. F., Wofsy, S. C., and Rocha, H. R.: The effects of biomass burning aerosols  
1005 and clouds on the CO<sub>2</sub> flux in Amazonia, *Tellus Series B-Chemical and Physical*  
1006 *Meteorology*, 59, 338-349, doi:10.1111/j.1600-0889.2007.00270.x, 2007.

1007 Pacifico, F., Folberth, G. A., Sitch, S., Haywood, J. M., Rizzo, L. V., Malavelle, F. F., and  
1008 Artaxo, P.: Biomass burning related ozone damage on vegetation over the Amazon forest:  
1009 a model sensitivity study, *Atmospheric Chemistry and Physics*, 15, 2791-2804,  
1010 doi:10.5194/acp-15-2791-2015, 2015.

1011 Randerson, J. T., Liu, H., Flanner, M. G., Chambers, S. D., Jin, Y., Hess, P. G., Pfister, G.,  
1012 Mack, M. C., Treseder, K. K., Welp, L. R., Chapin, F. S., Harden, J. W., Goulden, M. L.,  
1013 Lyons, E., Neff, J. C., Schuur, E. A. G., and Zender, C. S.: The impact of boreal forest  
1014 fire on climate warming, *Science*, 314, 1130-1132, doi:10.1126/Science.1132075, 2006.

1015 Rap, A., Spracklen, D. V., Mercado, L., Reddington, C. L., Haywood, J. M., Ellis, R. J.,  
1016 Phillips, O. L., Artaxo, P., Bonal, D., Coupe, N. R., and Butt, N.: Fires increase Amazon  
1017 forest productivity through increases in diffuse radiation, *Geophysical Research Letters*,  
1018 42, 4654-4662, doi:10.1002/2015gl063719, 2015.

1019 Remer, L. A., Mattoo, S., Levy, R. C., and Munchak, L. A.: MODIS 3 km aerosol product:  
1020 algorithm and global perspective, *Atmospheric Measurement Techniques*, 6, 1829-1844,  
1021 doi:10.5194/amt-6-1829-2013, 2013.

1022 Rodenbeck, C., Houweling, S., Gloor, M., and Heimann, M.: CO<sub>2</sub> flux history 1982-2001  
1023 inferred from atmospheric data using a global inversion of atmospheric transport,  
1024 *Atmospheric Chemistry and Physics*, 3, 1919-1964, 2003.

1025 Schaefer, K., Collatz, G. J., Tans, P., Denning, A. S., Baker, I., Berry, J., Prihodko, L., Suits,  
1026 N., and Philpott, A.: Combined Simple Biosphere/Carnegie-Ames-Stanford Approach  
1027 terrestrial carbon cycle model, *J. Geophys. Res.*, 113, G03034,  
1028 doi:10.1029/2007jg000603, 2008.

1029 Schmidt, G. A., Kelley, M., Nazarenko, L., Ruedy, R., Russell, G. L., Aleinov, I., Bauer, M.,  
1030 Bauer, S. E., Bhat, M. K., Bleck, R., Canuto, V., Chen, Y. H., Cheng, Y., Clune, T. L.,  
1031 Del Genio, A., de Fainchtein, R., Faluvegi, G., Hansen, J. E., Healy, R. J., Kiang, N. Y.,  
1032 Koch, D., Lacis, A. A., LeGrande, A. N., Lerner, J., Lo, K. K., Matthews, E. E., Menon,  
1033 S., Miller, R. L., Oinas, V., Olosio, A. O., Perlwitz, J. P., Puma, M. J., Putman, W. M.,

1034 Rind, D., Romanou, A., Sato, M., Shindell, D. T., Sun, S., Syed, R. A., Tausnev, N.,  
1035 Tsigaridis, K., Unger, N., Voulgarakis, A., Yao, M. S., and Zhang, J. L.: Configuration  
1036 and assessment of the GISS ModelE2 contributions to the CMIP5 archive, *Journal of*  
1037 *Advances in Modeling Earth Systems*, 6, 141-184, doi:10.1002/2013ms000265, 2014.

1038 Shindell, D. T., Lamarque, J. F., Schulz, M., Flanner, M., Jiao, C., Chin, M., Young, P. J.,  
1039 Lee, Y. H., Rotstayn, L., Mahowald, N., Milly, G., Faluvegi, G., Balkanski, Y., Collins,  
1040 W. J., Conley, A. J., Dalsoren, S., Easter, R., Ghan, S., Horowitz, L., Liu, X., Myhre, G.,  
1041 Nagashima, T., Naik, V., Rumbold, S. T., Skeie, R., Sudo, K., Szopa, S., Takemura, T.,  
1042 Voulgarakis, A., Yoon, J. H., and Lo, F.: Radiative forcing in the ACCMIP historical and  
1043 future climate simulations, *Atmospheric Chemistry and Physics*, 13, 2939-2974, doi:10.5194/Acp-13-2939-2013, 2013a.

1045 Shindell, D. T., Pechony, O., Voulgarakis, A., Faluvegi, G., Nazarenko, L., Lamarque, J. F.,  
1046 Bowman, K., Milly, G., Kovari, B., Ruedy, R., and Schmidt, G. A.: Interactive ozone  
1047 and methane chemistry in GISS-E2 historical and future climate simulations,  
1048 *Atmospheric Chemistry and Physics*, 13, 2653-2689, doi:10.5194/Acp-13-2653-2013,  
1049 2013b.

1050 Sitch, S., Cox, P. M., Collins, W. J., and Huntingford, C.: Indirect radiative forcing of climate  
1051 change through ozone effects on the land-carbon sink, *Nature*, 448, 791-794,  
1052 doi:10.1038/Nature06059, 2007.

1053 Solomon, S., Qin, D., Manning, M., Chen, Z., Marquis, M., Averyt, K. B., Tignor, M., and  
1054 Miller, H. L.: *Climate Change 2007: Working Group I: The Physical Science Basis*,  
1055 Cambridge University Press, Cambridge, United Kingdom and New York, NY, USA,  
1056 2007.

1057 Spitters, C. J. T.: Separating the Diffuse and Direct Component of Global Radiation and Its  
1058 Implications for Modeling Canopy Photosynthesis .2. Calculation of Canopy  
1059 Photosynthesis, *Agricultural and Forest Meteorology*, 38, 231-242, doi:10.1016/0168-  
1060 1923(86)90061-4, 1986.

1061 Stocks, B. J., Mason, J. A., Todd, J. B., Bosch, E. M., Wotton, B. M., Amiro, B. D.,  
1062 Flannigan, M. D., Hirsch, K. G., Logan, K. A., Martell, D. L., and Skinner, W. R.: Large  
1063 forest fires in Canada, 1959-1997, *Journal of Geophysical Research*, 108, 8149,  
1064 doi:10.1029/2001jd000484, 2002.

1065 Strada, S., Unger, N., and Yue, X.: Observed aerosol-induced radiative effect on plant  
1066 productivity in the eastern United States, *Atmospheric Environment*, 122, 463-476,  
1067 doi:10.1016/j.atmosenv.2015.09.051, 2015.

1068 Tosca, M. G., Randerson, J. T., Zender, C. S., Flanner, M. G., and Rasch, P. J.: Do biomass  
1069 burning aerosols intensify drought in equatorial Asia during El Niño?, *Atmospheric*  
1070 *Chemistry and Physics*, 10, 3515-3528, doi:10.5194/acp-10-3515-2010, 2010.

1071 Turetsky, M. R., Kane, E. S., Harden, J. W., Ottmar, R. D., Manies, K. L., Hoy, E., and  
1072 Kasischke, E. S.: Recent acceleration of biomass burning and carbon losses in Alaskan  
1073 forests and peatlands, *Nature Geoscience*, 4, 27-31, doi:10.1038/Ngeo1027, 2011.

1074 Tymstra, C., Flannigan, M. D., Armitage, O. B., and Logan, K.: Impact of climate change on  
1075 area burned in Alberta's boreal forest, *Int. J. Wildland Fire*, 16, 153-160,  
1076 doi:10.1071/Wf06084, 2007.

1077 Unger, N., Harper, K., Zheng, Y., Kiang, N. Y., Aleinov, I., Arneth, A., Schurgers, G.,  
 1078 Amelynck, C., Goldstein, A., Guenther, A., Heinesch, B., Hewitt, C. N., Karl, T.,  
 1079 Laffineur, Q., Langford, B., McKinney, K. A., Misztal, P., Potosnak, M., Rinne, J.,  
 1080 Pressley, S., Schoon, N., and Serça, D.: Photosynthesis-dependent isoprene emission  
 1081 from leaf to planet in a global carbon–chemistry–climate model, *Atmos. Chem. Phys.*, 13,  
 1082 17717-17791, doi:10.5194/acp-13-10243-2013, 2013.  
 1083 Vachon, F., Royer, A., Aube, M., Toubbe, B., O'Neill, N. T., and Teillet, P. M.: Remote  
 1084 sensing of aerosols over North American land surfaces from POLDER and MODIS  
 1085 measurements, *Atmospheric Environment*, 38, 3501-3515,  
 1086 doi:10.1016/j.atmosenv.2004.01.046, 2004.  
 1087 Val Martin, M., Kahn, R. A., Logan, J. A., Paugam, R., Wooster, M., and Ichoku, C.: Space-  
 1088 based observational constraints for 1-D plume rise models, *J. Geophys. Res.*, 117,  
 1089 D22204, doi:10.1029/2012JD018370, 2012.  
 1090 van der Werf, G. R., Randerson, J. T., Giglio, L., Collatz, G. J., Mu, M., Kasibhatla, P. S.,  
 1091 Morton, D. C., DeFries, R. S., Jin, Y., and van Leeuwen, T. T.: Global fire emissions and  
 1092 the contribution of deforestation, savanna, forest, agricultural, and peat fires (1997-2009),  
 1093 *Atmospheric Chemistry and Physics*, 10, 11707-11735, doi:10.5194/Acp-10-11707-2010,  
 1094 2010.  
 1095 van Vuuren, D. P., Edmonds, J., Kainuma, M., Riahi, K., Thomson, A., Hibbard, K., Hurtt, G.  
 1096 C., Kram, T., Krey, V., Lamarque, J. F., Masui, T., Meinshausen, M., Nakicenovic, N.,  
 1097 Smith, S. J., and Rose, S. K.: The representative concentration pathways: an overview,  
 1098 *Climatic Change*, 109, 5-31, doi:10.1007/s10584-011-0148-z, 2011.  
 1099 Wang, X., Thompson, D. K., Marshall, G. A., Tymstra, C., Carr, R., and Flannigan, M. D.:  
 1100 Increasing frequency of extreme fire weather in Canada with climate change, *Climatic*  
 1101 *Change*, 130, 573-586, doi:10.1007/s10584-015-1375-5, 2015.  
 1102 Wang, X. L., Parisien, M. A., Taylor, S. W., Perrakis, D. D. B., Little, J., and Flannigan, M.  
 1103 D.: Future burn probability in south-central British Columbia, *International Journal of*  
 1104 *Wildland Fire*, 25, 200-212, doi:10.1071/Wf15091, 2016.  
 1105 Wild, M., Folini, D., Schar, C., Loeb, N., Dutton, E. G., and Konig-Langlo, G.: The global  
 1106 energy balance from a surface perspective, *Climate Dynamics*, 40, 3107-3134,  
 1107 doi:10.1007/s00382-012-1569-8, 2013.  
 1108 Wittig, V. E., Ainsworth, E. A., and Long, S. P.: To what extent do current and projected  
 1109 increases in surface ozone affect photosynthesis and stomatal conductance of trees? A  
 1110 meta-analytic review of the last 3 decades of experiments, *Plant Cell and Environment*,  
 1111 30, 1150-1162, doi:10.1111/J.1365-3040.2007.01717.X, 2007.  
 1112 Wotawa, G., and Trainer, M.: The influence of Canadian forest fires on pollutant  
 1113 concentrations in the United States, *Science*, 288, 324-328, 2000.  
 1114 Wotton, B. M., Nock, C. A., and Flannigan, M. D.: Forest fire occurrence and climate change  
 1115 in Canada, *International Journal of Wildland Fire*, 19, 253-271, doi:10.1071/Wf09002,  
 1116 2010.  
 1117 Yue, X., Mickley, L. J., Logan, J. A., and Kaplan, J. O.: Ensemble projections of wildfire  
 1118 activity and carbonaceous aerosol concentrations over the western United States in the

1119 mid-21st century, *Atmos. Environ.*, 77, 767-780, doi:10.1016/J.Atmosenv.2013.06.003,  
1120 2013.

1121 Yue, X., and Unger, N.: Ozone vegetation damage effects on gross primary productivity in  
1122 the United States, *Atmospheric Chemistry and Physics*, 14, 9137-9153, doi:10.5194/acp-  
1123 14-9137-2014, 2014.

1124 Yue, X., Mickley, L. J., Logan, J. A., Hudman, R. C., Martin, M. V., and Yantosca, R. M.:  
1125 Impact of 2050 climate change on North American wildfire: consequences for ozone air  
1126 quality, *Atmospheric Chemistry and Physics*, 15, 10033-10055, doi:10.5194/acp-15-  
1127 10033-2015, 2015.

1128 Yue, X., and Unger, N.: The Yale Interactive terrestrial Biosphere model version 1.0:  
1129 description, evaluation and implementation into NASA GISS ModelE2, *Geoscientific  
1130 Model Development*, 8, 2399-2417, doi:10.5194/gmd-8-2399-2015, 2015.

1131 Yue, X., Keenan, T. F., Munger, W., and Unger, N.: Limited effect of ozone reductions on  
1132 the 20-year photosynthesis trend at Harvard forest, *Global Change Biology*, 22, 3750-  
1133 3759, doi:10.1111/gcb.13300, 2016.

1134 Yue, X., Unger, N., Harper, K., Xia, X., Liao, H., Zhu, T., Xiao, J., Feng, Z., and Li, J.:  
1135 Ozone and haze pollution weakens net primary productivity in China, *Atmospheric  
1136 Chemistry and Physics*, 17, 6073-6089, doi:10.5194/acp-17-6073-2017, 2017.

1137 Zhao, Z., Kooperman, G. J., Pritchard, M. S., Russell, L. M., and Somerville, R. C. J.:  
1138 Investigating impacts of forest fires in Alaska and western Canada on regional weather  
1139 over the northeastern United States using CAM5 global simulations to constrain  
1140 transport to a WRF-Chem regional domain, *Journal of Geophysical Research*, 119, 7515-  
1141 7536, doi:10.1002/2013jd020973, 2014.

1142 Zu, K., Tao, G., Long, C., Goodman, J., and Valberg, P.: Long-range fine particulate matter  
1143 from the 2002 Quebec forest fires and daily mortality in Greater Boston and New York  
1144 City, *Air Quality Atmosphere and Health*, 9, 213-221, doi:10.1007/s11869-015-0332-9,  
1145 2016.

1146  
1147 |

1148  
1149  
1150  
1151  
1152  
1153  
1154  
1155  
1156  
1157  
1158  
1159  
1160  
1161  
1162  
1163  
1164  
1165  
1166  
1167  
1168  
1169  
1170  
1171  
1172  
1173  
1174  
1175  
1176  
1177  
1178

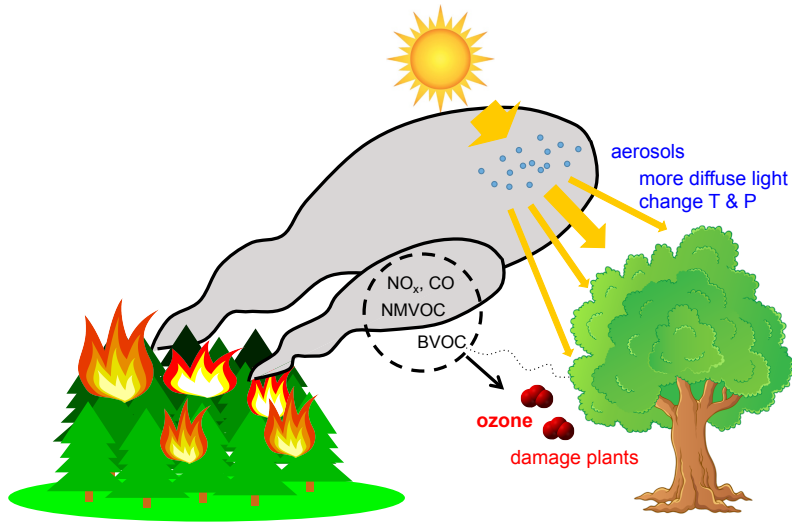
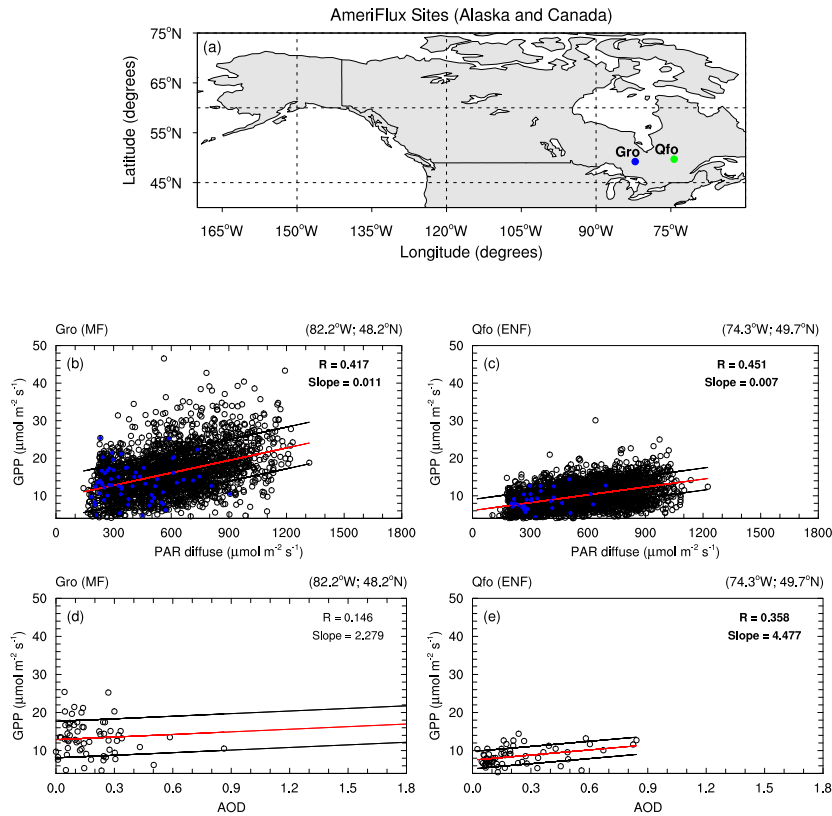


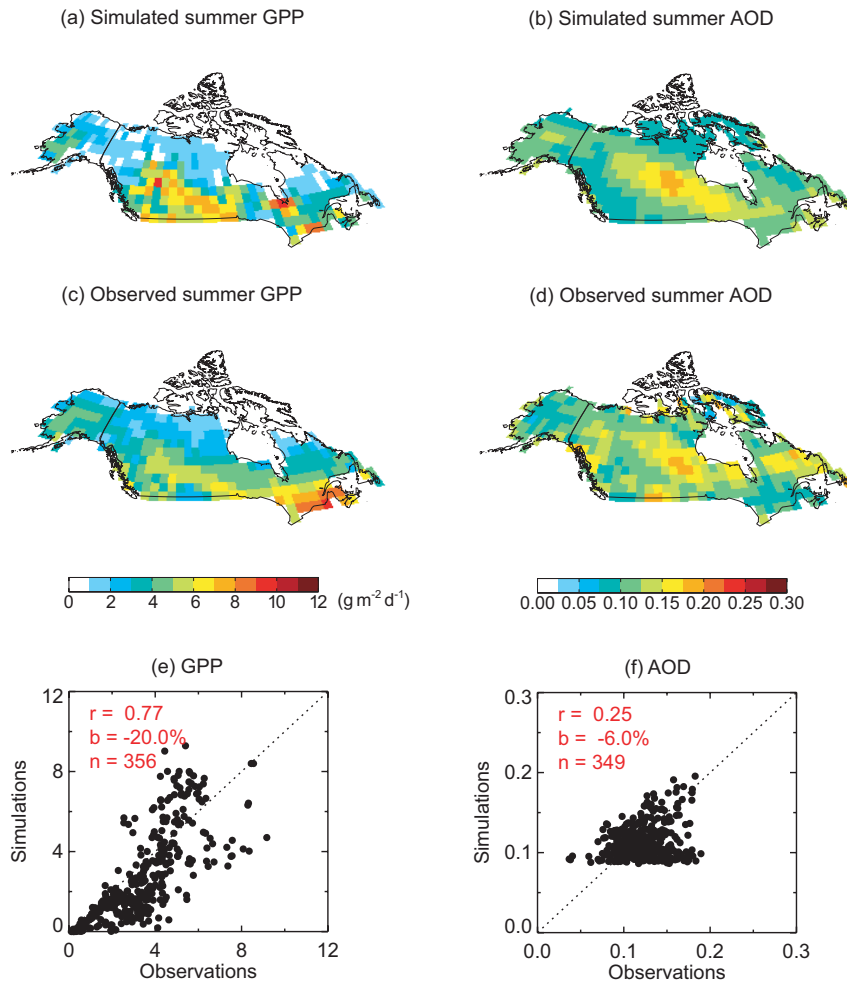
**Figure 1.** Illustration of atmospheric chemistry and physics, and biospheric processes investigated in the study. Carbonaceous aerosols from fire plumes increase diffuse light and change temperature and precipitation, influencing vegetation photosynthesis. Ozone generated photochemically from fire-emitted precursors (NO<sub>x</sub>, CO, and non-methane volatile organic compound (NMVOC)) and associated BVOC changes causes direct damage to plant photosynthesis.



1180  
 1181 **Figure 2.** Relationships between (b, c) GPP and diffuse PAR and (d, e) GPP and MODIS  
 1182 AOD at (a) two boreal sites: Groundhog River (Gro) and Quebec Mature Boreal Forest Site  
 1183 (Qfo). The two sites are from the AmeriFlux network in Canada and are dominated by mixed  
 1184 forest (MF at Gro) and evergreen needleleaf forest (ENF at Qfo) (Table 1). Data cover  
 1185 summer days (June-August). AmeriFlux diffuse PAR and GPP (in  $\mu\text{mol m}^{-2} \text{s}^{-1}$ ) are half-  
 1186 hourly observations (10:00-14:00 LT). Instantaneous MODIS Aqua and Terra 3-km AOD are  
 1187 selected in a time span centered on AmeriFlux record time. For each plot: the red line  
 1188 indicates the regression line, black lines depict the 1- $\sigma$  interval; the regression slope and  
 1189 correlation coefficient are both included for each site (in bold if statistically significant at 95%  
 1190 confidence level). Blue dots in (b, c) show instants when MODIS Aqua and Terra 3-km  
 1191 AODs overlap AmeriFlux data.

1192  
 1193

1194  
1195



1196  
1197

1198 **Figure 3.** Evaluation of simulated summer (a) GPP and (b) AOD at 550 nm with (c, d)  
1199 observations. Simulation results are from F10AERO (Table 1). Each point on the (e, f) scatter  
1200 plot represents one grid square in boreal North America. The number of points (n),  
1201 correlation coefficient (r), and relative bias (b) for the evaluation are presented on the plot.

1202  
1203



1204  
1205  
1206  
1207  
1208  
1209  
1210  
1211  
1212  
1213  
1214  
1215  
1216  
1217  
1218  
1219  
1220  
1221  
1222  
1223  
1224  
1225  
1226  
1227  
1228  
1229  
1230  
1231  
1232  
1233  
1234  
1235  
1236  
1237  
1238  
1239  
1240  
1241  
1242  
1243  
1244  
1245  
1246  
1247

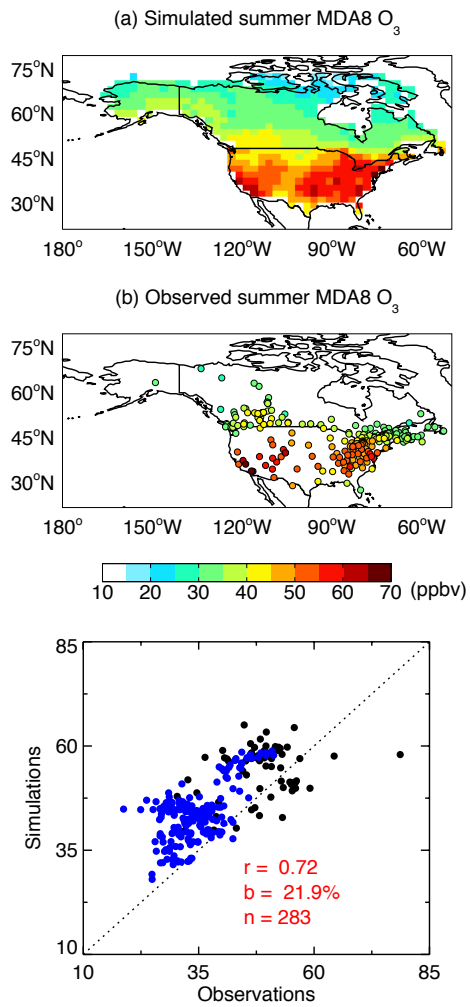
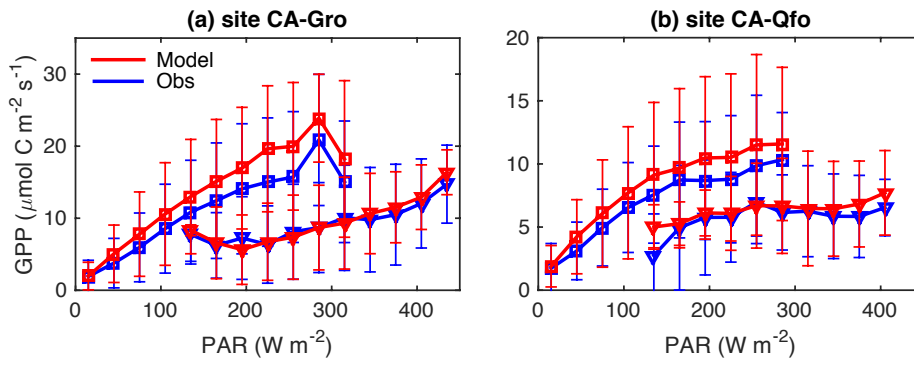


**Figure 4.** Evaluation of simulated summer surface maximum daily 8-hour average [O<sub>3</sub>] with observations for 2008-2012. Observations are collected from 81 U.S. sites at the Clean Air Status and Trends Network (CASTNET) and 202 Canadian sites at the National Air Pollution Surveillance (NAPS) program. The number of points (n), correlation coefficient (r), and mean bias (b) for the evaluation are presented on the plot. Values over Canada and Alaska are denoted with blue points.

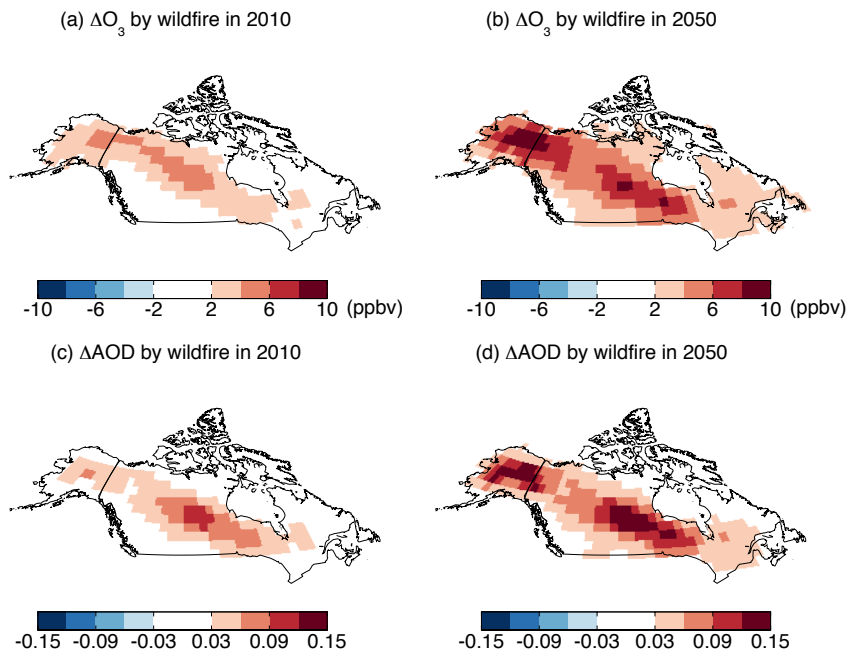
1248  
1249  
1250



1251  
1252  
1253  
1254  
1255  
1256  
1257  
1258

**Figure 5.** Observed (blue) and simulated (red) response of GPP to diffuse (square) and direct (triangle) PAR at boreal sites (a) CA-Gro (2004-2013) and (b) CA-Qfo (2004-2010). Observations and simulations are split into ‘diffuse’ and ‘direct’ conditions if the diffuse fraction is  $>0.8$  and  $<0.2$ , respectively. Data points are then averaged over PAR bins of  $30 \text{ W m}^{-2}$  with error bars indicating one standard deviation of GPP for each bin.

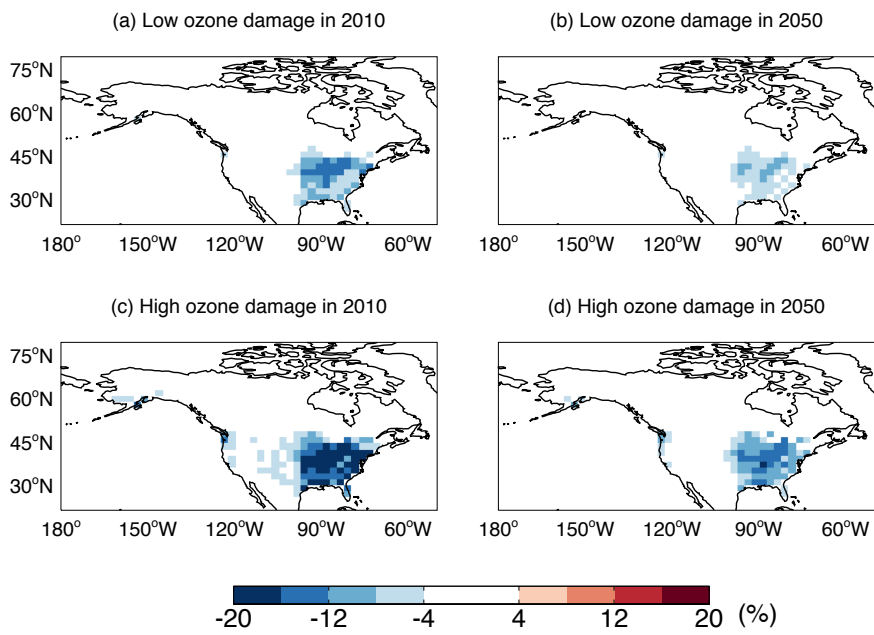
1259  
1260



1261  
1262 **Figure 6.** Changes in summer (a, b)  $[O_3]$  and (c, d) AOD at 550 nm induced by wildfire  
1263 emissions in (a, c) the 2010s and (b, d) the 2050s over boreal North America. Only  
1264 significant changes ( $p < 0.05$ ) are shown.

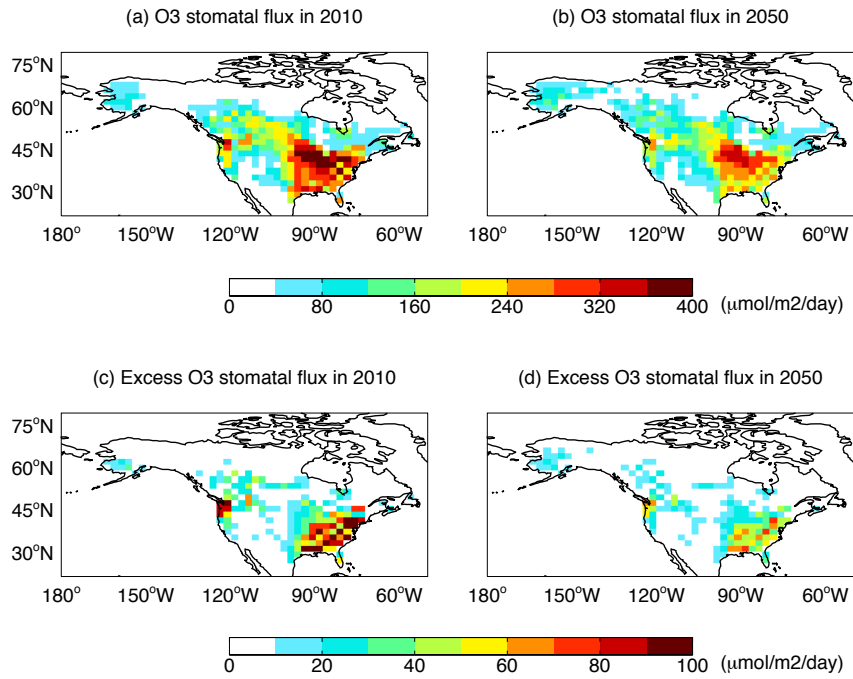
1265  
1266

1267  
1268



1269 **Figure 7.** Simulated O<sub>3</sub> damages to summer GPP in North America. Results shown are from  
1270 simulations with (a, b) low and (c, d) high O<sub>3</sub> sensitivities for (a, c) 2010 and (b, d) 2050.  
1271 Simulated [O<sub>3</sub>] includes contributions from both wildfire and non-fire emissions. Results for  
1272 2010 are derived as  $(F10O3/F10CTRL-1) \times 100\%$ . Results for 2050 are derived as  
1273  $(F50O3/F50CTRL-1) \times 100\%$ .  
1274

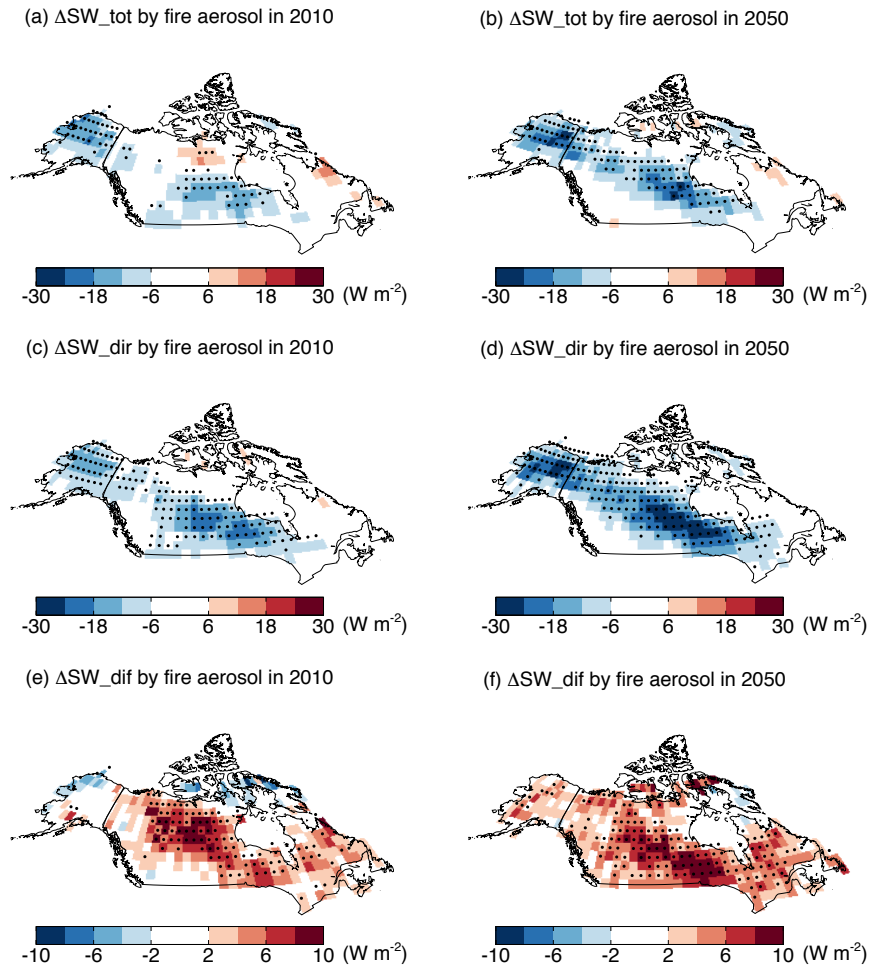
1275  
1276  
1277



1279  
 1280 **Figure 8.** Simulated summertime O<sub>3</sub> stomatal fluxes in boreal North America. Results shown  
 1281 are the (a, b) mean and (c, d) excess flux at (a, c) 2010 and (b, d) 2050. Simulated [O<sub>3</sub>]  
 1282 includes contributions from both wildfire and non-fire emissions. Excess O<sub>3</sub> stomatal flux is  
 1283 calculated as the difference between the stomatal flux and a PFT-specific threshold as defined  
 1284 in Sitch et al. (2007).

1285  
 1286

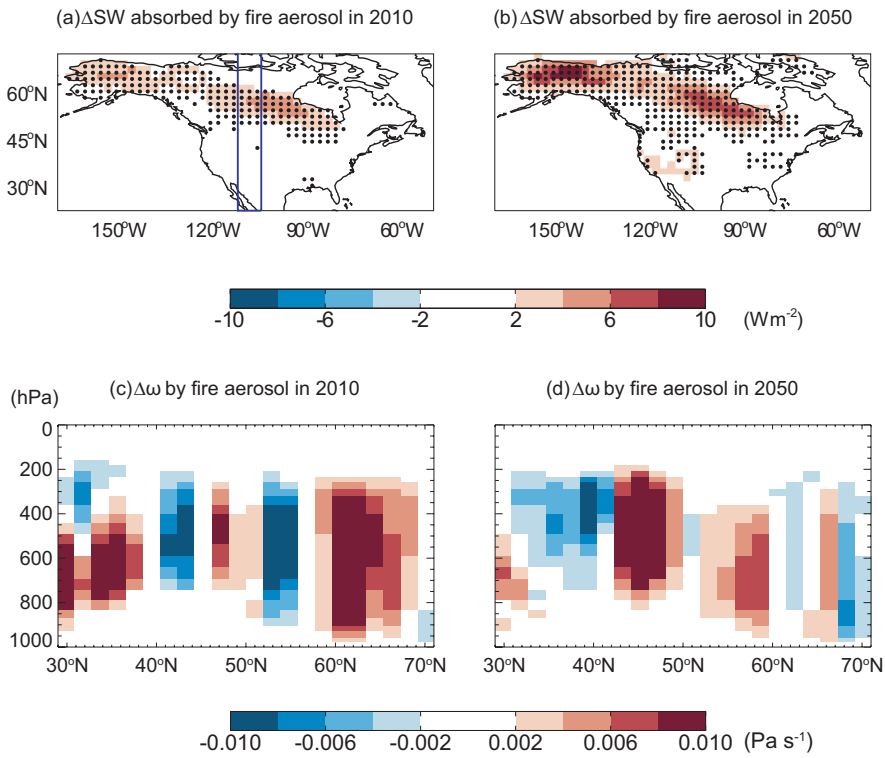
1287  
1288



1289  
1290  
1291  
1292  
1293  
1294  
1295  
1296  
1297  
1298

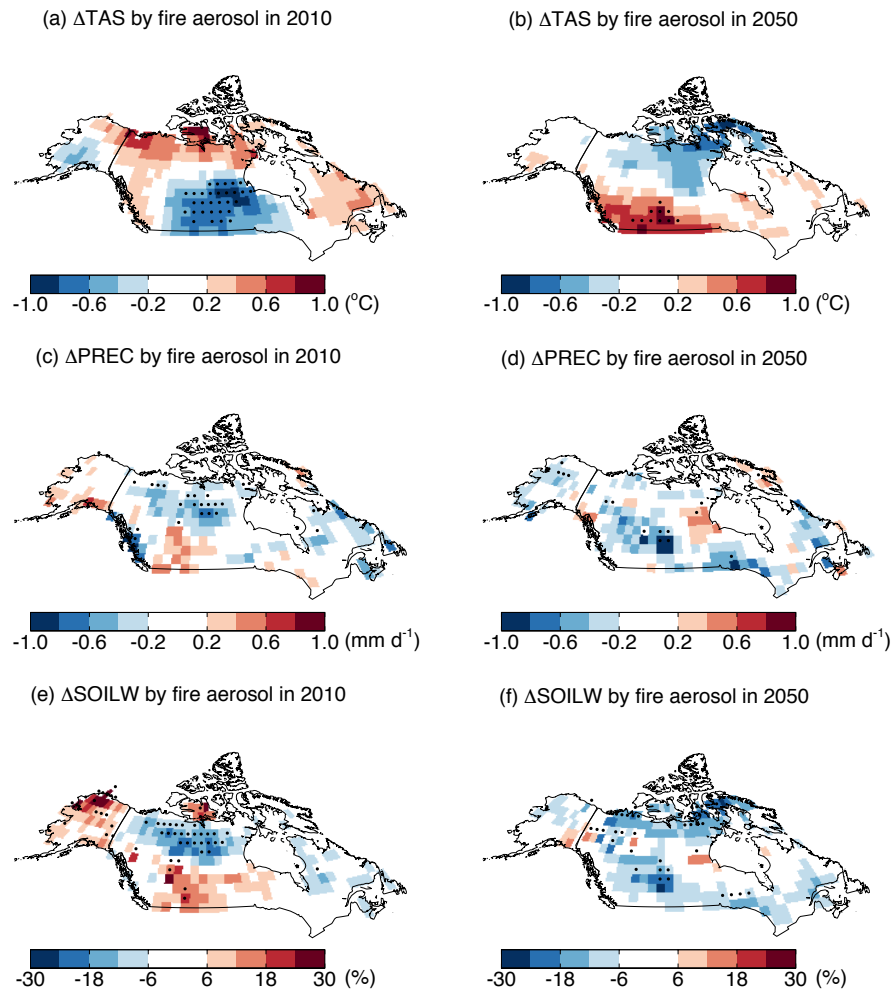
**Figure 9.** Changes in surface radiative fluxes induced by wildfire aerosols in boreal North America. Results shown are for the changes in summertime (June-August) (a, b) total, (c, d) direct, and (e, f) diffuse solar radiation at surface caused by aerosols from wildfire emissions at (a, c, e) present day and (b, d, f) midcentury. Significant changes ( $p < 0.05$ ) are marked with black dots. Results for 2010 are calculated as (F10AERO - F10CTRL). Results for 2050 are calculated as (F50AERO - F50CTRL).

1299  
1300



1301  
1302  
1303  
1304  
1305  
1306  
1307  
1308  
1309  
1310  
1311  
1312

**Figure 10.** Predicted (a, b) absorption of shortwave radiation and (c, d) perturbations in vertical velocity by wildfire aerosols at (a, c) present day and (b, d) midcentury. The absorption of shortwave radiation is calculated as the differences of radiative perturbations between top of atmosphere and surface. Vertical velocity is calculated as the longitudinal average between 105°W and 112.5°W (two blue lines in a). Positive (negative) values indicate descending (rising) motion. Results for the 2010s are calculated as (F10AERO - F10CTRL). Results for the 2050s are calculated as (F50AERO - F50CTRL). Significant changes ( $p < 0.05$ ) in (a, b) are indicated as black points.



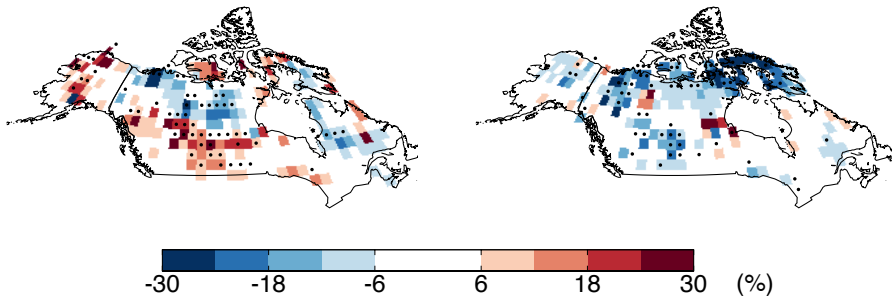
1313  
 1314 **Figure 11.** Predicted changes in summertime (a, b) surface air temperature, (c, d)  
 1315 precipitation, and (e, f) soil water content at surface caused by aerosols from wildfire  
 1316 emissions at (a, c, e) present day and (b, d, f) midcentury. Results for temperature and  
 1317 precipitation are shown as absolute changes. Results for soil water are shown as relative  
 1318 changes. Results for the 2010s are calculated as (F10AERO - F10CTRL). Results for the  
 1319 2050s are calculated as (F50AERO - F50CTRL). Significant changes ( $p < 0.05$ ) are marked  
 1320 with black dots.  
 1321



1322  
1323

(a)  $\Delta$ NPP by fire aerosol in 2010

1324  
(b)  $\Delta$ NPP by fire aerosol in 2050



1325  
1326  
1327

1328 **Figure 12.** Predicted percentage changes in summer NPP caused by wildfire aerosols at (a)  
1329 present day and (b) midcentury. Results for the 2010s are calculated as  $(F10AERO/F10CTRL$   
1330  $- 1) \times 100\%$ . Results for the 2050s are calculated as  $(F50AERO/F50CTRL - 1) \times 100\%$ .  
1331 Significant changes ( $p < 0.05$ ) are marked with black dots.

1332  
1333  
1334  
1335